

# Guide your favorite protein sequence generative model

Junhao Xiong<sup>1†</sup>, Hunter Nisonoff<sup>1†</sup>, Maria Lukarska<sup>3,4,5†</sup>,  
Ishan Gaur<sup>1†</sup>, Luke M. Oltrogge<sup>3,4,5</sup>, David F. Savage<sup>3,4,5\*</sup>,  
Jennifer Listgarten<sup>1,2\*</sup>

<sup>1</sup>Department of Electrical Engineering & Computer Sciences, University of California, Berkeley, Berkeley, 94720, CA, USA.

<sup>2</sup>Center for Computational Biology, University of California, Berkeley, Berkeley, 94720, CA, USA.

<sup>3</sup>Department of Molecular and Cell Biology, University of California, Berkeley, Berkeley, 94720, CA, USA.

<sup>4</sup>Innovative Genomics Institute, University of California, Berkeley, Berkeley, 94720, CA, USA.

<sup>5</sup>Howard Hughes Medical Institute, University of California, Berkeley, Berkeley, 94720, CA, USA.

\*Corresponding author(s). E-mail(s): [savage@berkeley.edu](mailto:savage@berkeley.edu);  
[jennl@berkeley.edu](mailto:jennl@berkeley.edu);

†These authors contributed equally to this work.

## Abstract

Generative machine learning models on sequences are transforming protein engineering. However, no principled framework exists for conditioning these models on auxiliary information, such as experimental data, in a plug-and-play manner. Herein, we present ProteinGuide—a principled and general method for conditioning—by unifying a broad class of protein generative models under a single framework. We demonstrate the applicability of ProteinGuide by guiding two protein generative models, ProteinMPNN and ESM3, to generate amino acid and structure token sequences, conditioned on several user-specified properties such as enhanced stability, enzyme classes, and CATH-labeled folds. We also used ProteinGuide with inverse folding models and our own experimental assay to design adenine base editor sequences for high activity.

Generative models are enabling protein engineers to create bespoke proteins for therapeutic, agricultural and environmental uses [1–3]. The outcome of any AI-based protein engineering approach is to ultimately specify a protein sequence, or a set of such sequences, even when designed by way of structure. For example, one might first use a backbone structure generative model such as RFdiffusion [2], Chroma [3], or ESM3 [4], followed by use of a backbone-conditioned generative model on sequences (also called an inverse-folding model), such as ProteinMPNN [1] or ESM-IF1 [5], to generate sequences likely to fold into the specified backbones. Alternatively, one might forgo generating a backbone structure intermediary and instead generate sequences directly from an “evolutionary” sequence-only model such as ESM3 [4], ProGen [6], EvoDiff [7], DPLM [8] and others [9, 10]. In all cases, the final step employs a generative model of sequences.

A key ingredient missing from the current protein engineering AI menu is the plug-and-play ability to *post hoc* “guide” sequence generative models toward properties of interest, because the technical underpinnings to do so have remained elusive. By guide, we mean, formally, to condition the probability distribution encoded by an existing generative model,  $p(x)$ , on newly-desired properties of interest,  $p(y \in Y|x)$ , so as to be able to generate (*i.e.*, sample) sequences from the desired conditional distribution,  $x \sim p(x|y \in Y)$ . Importantly, we want to condition in a plug-and-play manner, meaning that we want to avoid re-training the existing generative model, instead modulating how we sample from it with an auxiliary model, such as a property predictive model. Although it is currently possible to re-train generative models to achieve property conditioning [11, 12], the plug-and-play characteristics of *guidance* would enable everyday users to readily adapt existing large, expensive-to-train models of interest to suit their needs, on-the-fly [13–15].<sup>1</sup>

For example, one may want to guide an inverse-folding model to produce proteins with greater solubility than the model naturally generates, or to produce proteins more likely to bind a particular target, and so forth. Perhaps more importantly, one might want to guide a model using newly acquired experimental measurements, such as catalytic activity for a desired reaction—that is, integrate experimental data in a statistically coherent manner with an existing generative model, without re-training the existing model. Such an ability would enable training-efficient iterative cycles of design, build, test, and learn—a process where experimental feedback guides subsequent AI-based design rounds.

We recently showed for the first time how to correctly and tractably perform guidance for two specific classes of generative models, diffusion and flow matching, on discrete state-spaces [16]. Discrete state-spaces include not only sequences of amino acid, DNA and RNA, but also SMILES strings, graphs, language tokens, structure tokens, or any object represented by a sequence of discrete tokens. Herein, we build on this work by i) generalizing our guidance method to two more commonly-used classes of generative models for discrete spaces, namely, a large class of Masked Language Models (MLMs) such as ESM3, and any-order autoregressive models (AO-ARMs) such as ProteinMPNN, yielding our new method, ProteinGuide, ii) illustrating *in silico*

---

<sup>1</sup>Herein, we use the term “guide” and “guidance” to refer to “predictor guidance” in Nisonoff et al. [16]. Interested readers can also find how to perform predictor-free guidance in that same work.

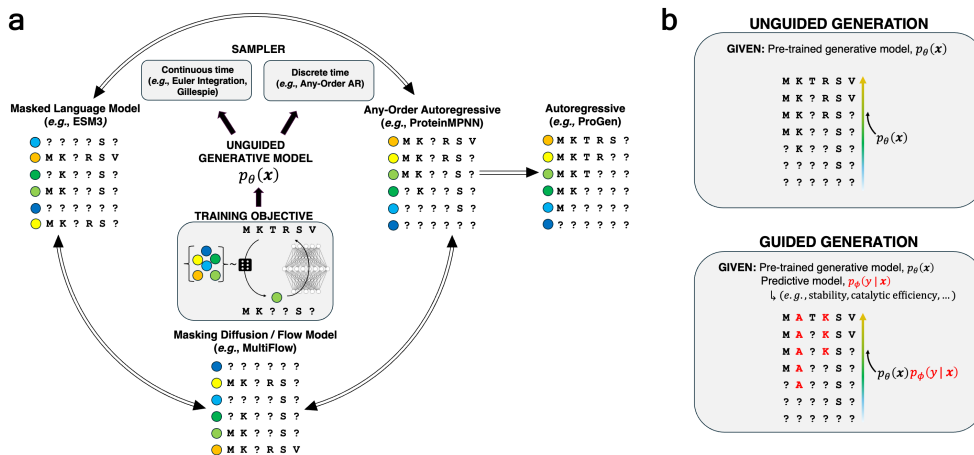


**Fig. 1: Equivalence between classes of generative models enables guidance with ProteinGuide.** **a.** Schematic showing how Masked Language Models (*e.g.*, ESM3) and any-order autoregressive models (*e.g.*, ProteinMPNN) can be viewed through the lens of masking diffusion/flow models. This interpretation enables generalization of our guidance method [16] to obtain ProteinGuide. Masking of one sequence position is denoted with the symbol “?”; colored dots help to visually tag individual sequences. The sequence being masked during training is M K R S V T;  $p_{\theta}(\mathbf{x})$  denotes the pre-trained generative model. The shared training objective involves randomly masking out parts of the sequence and then predicting the masked sequence given the remaining unmasked context, over different masking rates denoted by more or fewer “?” in a sequence. **b.** Contrasting unguided generation with guided generation by way of ProteinGuide. A sequence is denoted,  $\mathbf{x}$ , the pre-trained generative model is denoted  $p_{\theta}(\mathbf{x})$ ;  $y$  denotes a property of interest that we seek to guide toward using predictive model  $p_{\phi}(y | \mathbf{x})$ . When guiding, we coherently blend information from the predictive model with that of the pre-trained model in a statistically correct manner. Red letters indicate mutations that are introduced when guiding with the predictive model, and not seen when generating in an unguided manner.

application of ProteinGuide to representative use cases in protein engineering, and iii) applying ProteinGuide to obtain adenine base editors showing enhanced activity experimentally compared to the unguided model.

The essential technical formalism required to derive ProteinGuide, namely to generalize guidance in Nisonoff et al. [16] to MLMs and AO-ARMs, is the strong connection between these models and diffusion/flow matching models. Although conceptually diffusion/flow matching models, MLMs, and AO-ARMs seem to be quite different, it turns out that the loss functions used for training them are equivalent (Fig. 1a

and Methods).<sup>2</sup> Moreover, we show that sampling from a diffusion/flow matching model can be accomplished more simply, yet exactly, by sampling from a corresponding, trivial-to-construct AO-ARM (Methods). Altogether then, we can view a trained MLM or AO-ARM as a diffusion model on a discrete state-space, allowing us to leverage our earlier guidance method [16] for these models (Fig. 1b and Methods). While connections between these training objectives has been previously noted [19–23], the practical utility of this observation has been unclear. Herein, we show that this connection enables a general framework for guiding a broad class of models. Note that for autoregressive (AR) models, one can use FUDGE [24] for guidance, which can be viewed as a special case of ProteinGuide for the case of AR models. More detailed discussion of related work can be found in the Methods.

To illustrate the potential of ProteinGuide, we applied it, *in silico*, to three tasks, using two representative, well-known protein generative models, ProteinMPNN and ESM3. In our first task, we trained a regression model on experimental stability measurements [25] with which to guide ProteinMPNN to generate amino acid sequences encoding proteins that are more stable than what ProteinMPNN would do on its own (Fig. 2a). By employing guidance, we do so in a plug-and-play manner, rather than by re-training the inverse folding model [11]. In our second task, we guide ESM3 to re-design enzyme sequences predicted to belong to specific enzyme classes, based on a published classifier, CLEAN, for enzyme commission number (Fig. 2b) [17]. Our re-design task spans *de novo* design (starting with a 100% masked sequence), to 50% re-design, wherein half the sequence is masked out at random before generation, and the rest is held constant. In our third task, we demonstrate the generality of ProteinGuide beyond amino acid sequences, to structure tokens. In particular, we guide ESM3 to generate backbone structures (as tokens) with specified CATH fold class labels [26], by way of a classifier we trained on CATH data (Fig. 2c). Although ESM3 was trained to condition on free-form function word tokens, ProteinGuide offers a complementary, plug-and-play approach to conditioning on any property for which we have a predictive model (classifier or regressor), and so is not limited to conditioning on representations or data chosen at the time of ESM3 training. Across these three tasks, we observed that guidance, as expected, led to desired conditioning (Fig. 2a-c). Also, as expected, guiding ESM3 with rare CATH classes (which includes finer-grained CATH level labels) was more challenging—that is, had lower success rates. The quality of generated structures should improve concomitantly with improved backbone generative models, independent of guidance.

Finally, we used ProteinGuide to engineer an adenine base editor for high activity (Fig. 2d). ABEs are a class of CRISPR effectors that can introduce single nucleotide changes in the DNA [27]. We started with the wild-type TadA sequence (an ABE) which is known to have very low, but detectable activity [28] and used two models, an in-house flow-matching inverse folding model, FMIF [16], and ESM3, to jointly generate one library of 2,000 variants. We next estimated the activity of these variants by their enrichment in a bacterial selection assay based on the restoration of an inactive antibiotic resistance upon base editing (see Methods). Then we trained a classifier on

---

<sup>2</sup>For MLMs, the equivalence holds when the masking rate at training time covers fully masked, fully unmasked, and everything in between, such as for ESM3 (see Methods).

these data to predict high- vs. low-activity variants. Lastly, we applied ProteinGuide to design a second library of 2,000 sequences to be enriched for high activity relative to the first library. We found that the majority of the ProteinGuided variants in the second round had higher activities (mean log enrichment  $0.66 \pm 0.02$ ) than the first round library (mean log enrichment  $-0.28 \pm 0.01$ ). Furthermore, the second round library revealed variants that were more active than any seen in the first round library (Fig. 2e).

In conclusion, we introduced ProteinGuide, a broadly applicable framework that enables conditioning of pre-trained protein generative models on any property of interest that can be encoded in a predictive model, without having to re-train the pre-trained model. An important application enabled by our method is to incorporate feedback from experimental measurements into the generative process.

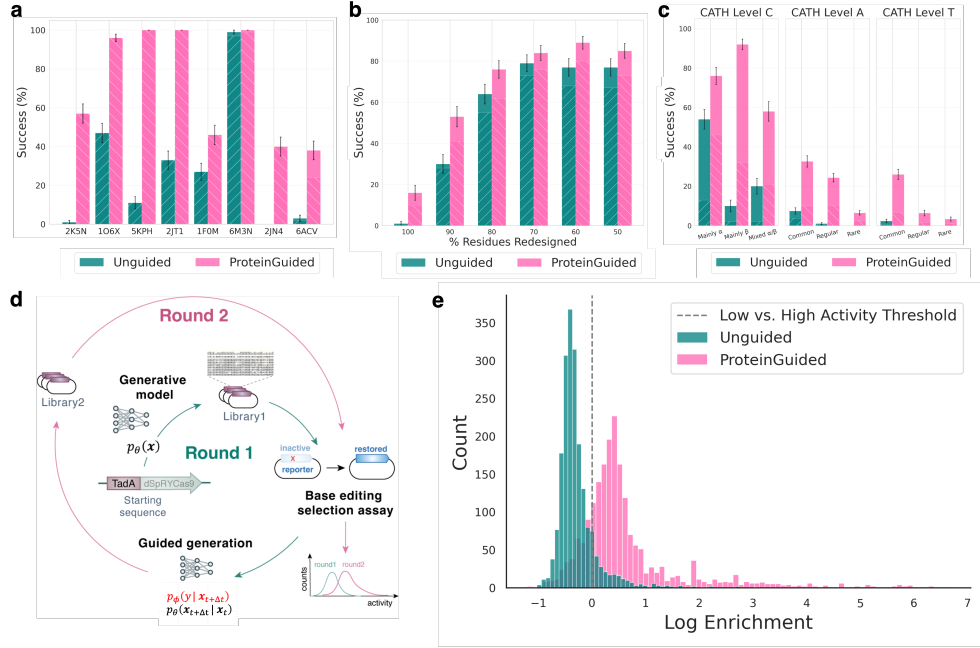


**Fig. 2: In silico and experimental demonstration of ProteinGuide.** **a.** Generating structure-conditioned protein sequences from ProteinMPNN without guidance (teal) and with ProteinGuide for stability (pink), across eight proteins (horizontal axis). The height of each bar represents the percentage of sequences predicted to be at least as stable as wild type ( $\Delta\Delta G \leq 0$ ), while the hatched sub-portion indicates the fraction of those stable sequences that are also predicted to correctly fold into the desired structure ( $\text{RMSD} \leq 2\text{\AA}$ ). Error bars on all panels represent standard errors of proportions, calculated as  $\sqrt{p(1-p)/n}$ , where  $p$  is the empirical proportion of success and  $n$  is the sample size. **b.** Using ESM3 to re-design enzyme sequences without guidance (teal) and with ProteinGuide (pink). The % residues re-designed refers to how many residues (positions) of a randomly chosen enzyme sequence from the target class were masked for re-design. When all are masked (100%), the task becomes *de novo* design. Bar height indicates the percentage of generated samples classified by CLEAN [17] as being from the correct (specified) target enzyme class. The hatched sub-portion shows the fraction of correctly classified samples with median pLDDT  $> 0.8$ . **c.** Generating backbone structure tokens with ESM3 without guidance (teal), and with fold class ProteinGuided ESM3 (pink), across different CATH hierarchy levels. The height of each bar shows the percentage of structures correctly classified to their target fold class, while the hatched sub-portion indicates the subset that are also designable (self-consistency  $\text{RMSD} \leq 2\text{\AA}$ ). Results are grouped by CATH level. For level C, there are three classes: mainly  $\alpha$ , mainly  $\beta$ , and mixed  $\alpha/\beta$ . For level A and T, we grouped the classes for each level by their frequency of occurrence in the AFDB (Common, Regular, Rare) and calculated the metrics within each group following Geffner et al. [18]. **d.** Schematic representation of the ProteinGuide ABE experiment. In round 1 we diversified a 86-amino acid TadA region using two generative models, ESM3 and FMIF, and built a library of 2,000 variants (library 1) which was assayed in a bacterial selection strain. The estimated activities of the library members were used to train a classifier to ProteinGuide for a second round of designs. This second round, library 2, contained 2,000 sequences that were cloned and assayed (round 2) and the activities of the two libraries were compared. **e.** A histogram of the experimentally measured log enrichments for both library 1 (teal) and library 2 (pink). ProteinGuide was used to generate the round 2 library such that variants would be enriched for having high activity (predicted activity in log enrichment units larger than the gray dashed line).

## Acknowledgments

This work was funded in part by the the U.S. Department of Energy, Office of Science, Office of Biological and Environmental Research, Lawrence Livermore National Laboratory BioSecure SFA within the Secure Biosystems Design program (SCW1710), and also the Office of Naval Research (ONR) under grant N00014-23-1-2587. D.F.S. is an Investigator of the Howard Hughes Medical Institute, M.L. is a Life Science Research Fellow funded by Howard Hughes Medical Institute. For their assistance with Illumina sequencing we thank the Innovative Genomics Institute NGS facility, Netravathi Krishnappa and for nanopore and Sanger sequencing we thank the UC Berkeley DNA Sequencing Facility. We thank Hanlun Jiang, Antoine Koehl, Jianan Canal Li, and Flora Zhiqi Wang for helpful discussions.

# Methods

## Background on discrete state-space diffusion and flow models

While diffusion models were initially developed for continuous state-spaces [13, 15, 29], recent work has extended these frameworks to discrete domains such as text, molecular graphs, and protein sequences. These extensions enable generative modeling of inherently discrete data without requiring continuous relaxations. There are a number of works defining discrete-time diffusion processes in discrete spaces [19, 30]. They were later extended to continuous-time [31–33] leveraging the formulation of continuous-time Markov chains (CTMCs), which describe stochastic processes where a system transitions between discrete states over continuous time. The dynamics of a CTMC are fully determined by an initial distribution  $p(x_0)$  and transition rates  $R_t(x, \tilde{x})$  that specify the instantaneous probability of transitioning from state  $x$  to state  $\tilde{x}$  at time  $t$ :

$$p(x_{t+dt} = \tilde{x} | x_t = x) = \delta_{x, \tilde{x}} + R_t(x, \tilde{x})dt + O(dt^{1+\epsilon}). \quad (1)$$

As an example, Campbell et al. [31] defines a forward noising process by specifying a time-dependent “forward” rate matrix that gradually transforms the (unknown) data distribution into a reference distribution, such as a uniform distribution over amino acid sequences. A denoising model is then trained to reverse this process, learning rates that can transform the corrupted samples back to samples from the data distribution.

There are also a number of works that extend flow matching, which were originally developed for continuous state-spaces [34–36], to discrete state-spaces [37, 38], also leveraging CTMCs, but differ from diffusion models in how the CTMCs are defined, which also induce different training objectives. These models specify a conditional flow that defines how probability mass should move from a noise distribution to the data distribution. The model learns to generate samples by following the flow trajectories. Campbell et al. [37] show that the rates used in generative sampling can be obtained by training a neural network with parameters  $\theta$ ,  $p_\theta(x_1|x_t, t)$ , to approximate the true denoising distribution using the standard cross-entropy loss,

$$\mathcal{L}_{\text{FM}} = \mathbb{E}_{x_1 \sim p_{\text{data}}(x_1), t \sim p(t), x_t \sim p_{t|1}(x_t|x_1)} [\log p_\theta(x_1|x_t, t)], \quad (2)$$

where  $x_1$  is the clean data,  $p(t)$ , referred to as the noise schedule, is a distribution with full support on the interval  $[0, 1]$ , and  $x_t$  is the noised data sample from the forward noising process  $p_{t|1}(x_t|x_1)$ .<sup>3</sup> As shown in Campbell et al. [37], the cross entropy loss can be understood as a simplification to the ELBO used to train continuous-time discrete diffusion models [31]. Given such a trained denoising model  $p_\theta(x_1|x_t, t)$ , the (unconditional) rate matrix used in sampling is defined as

$$R_t^\theta(x_t, x_{t+dt}) = \mathbb{E}_{x_1 \sim p_\theta(x_1|x_t)} \left[ \vec{R}_t(x_{t+dt}, x_t|x_1) \right], \quad (3)$$

where  $\vec{R}_t(x_{t+dt}, x_t|x_1)$  is the forward noising rate matrix induced by  $p(x_t|x_1)$ .

---

<sup>3</sup>For all models, we follow the convention of flow-based models, where  $t = 1$  is the target (training) distribution, and  $t = 0$  is the noise distribution.

In practice, for computational tractability, an independent forward noising process is used for each dimension,  $i \in \{1, 2, \dots, D\}$ , of  $x_1$ . Campbell et al. [31, 37] show that in this setting, the reverse process also factorizes per dimension. Thus, the denoising model,  $p_\theta(x_1|x_t, t)$ , need only learn a factorized distribution of the clean data and the loss becomes

$$\mathcal{L}_{\text{FM}} = \mathbb{E}_{x_1 \sim p_{\text{data}}(x_1), t \sim p(t), x_t \sim p_{t|1}(x_t|x_1)} \left[ \log \prod_{i=1}^D p_\theta(x_1^i|x_t, t) \right]. \quad (4)$$

Similarly, the rate matrix can be expressed per dimension as

$$R_t^{\theta, i}(x_t, x_{t+dt}^i) = \mathbb{E}_{x_1^i \sim p_\theta(x_1^i|x_t, t)} \left[ \overrightarrow{R}_t^i(x_{t+dt}^i, x_t^i|x_1^i) \right], \quad (5)$$

where  $\overrightarrow{R}_t^i(x_{t+dt}^i, x_t^i|x_1^i)$  is the forward noising rate matrix applied to dimension  $i$ .

There are many methods for sampling from discrete state-space diffusion and flow models by integrating the learned rate matrices with numerical integration schemes [31, 37–39]. One simple approach is Euler integration with a discrete time step  $\Delta t$ , where transition probabilities are computed as  $p(x_{t+\Delta t} = \tilde{x}|x_t = x) = \delta_{x, \tilde{x}} + R_t(x, \tilde{x})\Delta t$  and new states are sampled categorically at each step. Alternative methods include Gillespie’s algorithm [40, 41] for exact simulation and  $\tau$ -leaping [31] for approximate sampling that allows multiple dimension to transition simultaneously. The flow matching formulation also introduces a stochasticity hyperparameter  $\eta$  that can be adjusted at inference time to control the randomness of the sampling path, which Campbell et al. [37] showed could improve sample quality.

A popular instantiation of both discrete state-spaces diffusion and flow models uses masking as the per-dimension noising process, where tokens in a sequence are progressively replaced with mask tokens during the forward process and the model learns to recover the original tokens during the reverse process. For example, the masking conditional flow can be defined as  $p^{\text{mask}}(x_t^i|x_1^i) = \text{Cat}(t\delta\{x_1^i, x_t^i\} + (1-t)\delta\{?, x_t^i\})$ , where  $\delta\{i, j\}$  is the Kronecker delta which is 1 when  $i = j$ , 0 otherwise, and “?” denotes a mask token. Campbell et al. [37] showed that under the masking noise process, the unconditional rate matrix used in sampling defined in Equation 5 simplifies to

$$R_t^{\theta, i}(x_t, x_{t+dt}^i) = \frac{p_\theta(x_1^i|x_t, t)}{1-t} \delta\{x_t^i, ?\}. \quad (6)$$

This formulation has connections to Masked Language Models and any-order autoregressive model, which we will describe in detail next.

## Unifying connections between generative models on discrete state-spaces

Connections among masked discrete diffusion models, Masked Language Models (MLM) and any-order autoregressive models (AO-ARM) were initially pointed out by Austin et al. [19] and Hoogeboom et al. [20]. Recent works [21–23, 37, 38] further

clarified these connections, including the connections to CTMC-based formulation of diffusion and flow models [31, 33, 37], and showed that the continuous-time ELBO used to train masked diffusion models is essentially a weighted sum of cross entropy losses predicting the masked states from unmasked positions, where the proportion of masked positions ranges from 0 (complete masking) to 1 (no masking). For particular choices of the noise schedules, these training objectives can be shown to be equivalent to the training objective of any-order autoregressive models [42], (generative) Masked Language Models [19], and discrete flow-matching models [37, 38] under a masking process. Since ESM3 [4] and ProteinMPNN [1] were trained under the MLM and AO-ARM objectives respectively, and owing to the sampling equivalency between AO-ARMs and diffusion models, we can view ESM3 and ProteinMPNN as discrete state-space diffusion and flow models, and sample from them as such, leveraging the generative rate matrices from Equation 3 induced by the trained denoising model,  $p_\theta(x_1|x_t)$ . This formulation not only provides a principled way to sample from these models, but also offers additional sampling flexibility, including, but not limited to, the usage of different noise schedules during sampling from those used during training, and corrector-sampling [37, 38], which have been shown to sometimes improve sampling results compared to prior heuristics [43] for sampling from generative Masked Language Models [38]. In addition, this formulation unlocks the capacity to condition the generative process via guidance, which we introduce in a later section.

Here, we provide a self-contained derivation of the equivalence between the loss functions of discrete flow matching, Masked Language Models, and any-order autoregressive models.

### Equivalence between flow matching loss on discrete state-space and masked language modeling

Recall from Equation 4 that the flow matching loss is

$$\mathcal{L}_{\text{FM}} = \mathbb{E}_{x_1 \sim p_{\text{data}}(x_1), t \sim p(t), x_t \sim p_{t|1}(x_t|x_1)} \left[ \log \prod_{i=1}^D p_\theta(x_1^i|x_t, t) \right]. \quad (7)$$

Our goal is to demonstrate that this loss function is equivalent to the loss function used by a class of Masked Language Models (MLMs), that we will refer to as “generative Masked Language Models”. The key distinction between generative Masked Language Models and their non-generative counterparts, is that during training, generative MLMs mask tokens with a masking probability,  $t \in [0, 1]$ , sampled from a distribution  $p(t)$  that has full support on the interval  $[0, 1]$ . This requirement is met by MLMs such as ESM3 [4], but, importantly, is not met by BERT-style MLMs such as ESM2 [44], since these models use a fixed percentage of tokens that are masked at each step. Letting  $x_t$  refer to the masked sequence, we have that the generative masked language modeling objective function is

$$\mathcal{L}_{\text{MLM}} = \mathbb{E}_{x_1 \sim p_{\text{data}}(x_1), t \sim p(t), x_t \sim p_{t|1}(x_t|x_1)} \left[ \log \prod_{i=1}^D p_\theta(x_1^i|x_t) \right], \quad (8)$$

where we can see that the key difference between Equation 8 and Equation 4 is that the latter has a denoising neural network with a dependence on  $t$ . We will now show that when a masking noise process is used for flow matching, the denoiser’s dependency on  $t$  can be dropped, making the two loss functions equivalent.

Let  $x_1 = (x_1^1, x_1^2, \dots, x_1^D)$  be our original sequence from the data distribution. For a masking noise process we define binary masking variables  $m_t^i \in \{0, 1\}$  for each position  $i$  at time  $t$ , where  $m_t^i = 1$  indicates token  $i$  is masked at time  $t$  and  $m_t^i = 0$  indicates token  $i$  is not masked at time  $t$ . Using ‘?’ to denote a masked state, the state  $x_t$  is then defined as:

$$x_t^i = \begin{cases} x_1^i & \text{if } m_t^i = 0 \\ ? & \text{if } m_t^i = 1. \end{cases} \quad (9)$$

Let us additionally define:

1.  $M_t = \{i : x_t^i = ?\}$  as the set of masked positions at time  $t$ .
2.  $U_t = \{i : x_t^i \neq ?\}$  as the set of unmasked positions.

For any position  $i \in U_t$ , we know with certainty that  $x_t^i = x_1^i$  by the definition of our forward process. The key observation is that the time variable  $t$  only influences which tokens are masked (the masking pattern), but once we observe  $x_t$ , we have complete information about which positions are masked and which are not. The time variable, therefore, provides no additional information needed to predict the clean data. Using a mathematical argument first proposed by Gat et al. [38], we can prove this as follows:

$$p(x_1 | x_t, t) = \frac{p(x_t, t | x_1)p(x_1)}{\sum_{\tilde{x}_1} p(x_t, t | \tilde{x}_1)p(\tilde{x}_1)} \quad (10)$$

$$= \frac{[\prod_{i \in M_t} (1-t) \prod_{i \in U_t} t] [\prod_{i \in U_t} \delta\{x_t^i, x_1^i\}] p(t)p(x_1)}{\sum_{\tilde{x}_1} [\prod_{i \in M_t} (1-t) \prod_{i \in U_t} t] [\prod_{i \in U_t} \delta\{x_t^i, \tilde{x}_1^i\}] p(t)p(\tilde{x}_1)} \quad (11)$$

$$= \frac{[\prod_{i \in U_t} \delta\{x_t^i, x_1^i\}] p(x_1)}{\sum_{\tilde{x}_1} [\prod_{i \in U_t} \delta\{x_t^i, \tilde{x}_1^i\}] p(\tilde{x}_1)} \quad (12)$$

$$= p(x_1 | x_t). \quad (13)$$

where Equation 11 uses the factorization over the dimensions and analyze separately the two cases of whether a position is masked or unmasked, and Equation 12 shows that  $p(x_1 | x_t, t)$  does not depend on  $t$ , giving us Equation 13. Thus, we can rewrite the masking flow matching loss function as:

$$\mathcal{L}_{\text{FM}} = \mathbb{E}_{x_1 \sim p_{\text{data}}(x_1), t \sim p(t), x_t \sim p_{t|1}(x_t|x_1)} \left[ \log \prod_{i=1}^D p_{\theta}(x_1^i | x_t, t) \right] \quad (14)$$

$$= \mathbb{E}_{x_1 \sim p_{\text{data}}(x_1), t \sim p(t), x_t \sim p_{t|1}(x_t|x_1)} \left[ \log \prod_{i=1}^D p_{\theta}(x_1^i | x_t) \right] \quad (15)$$

$$= \mathcal{L}_{\text{MLM}}. \quad (16)$$

## Equivalence between flow matching loss on discrete state-spaces and any-order autoregressive training

any-order autoregressive models (AO-ARM) differ from standard autoregressive models by training on arbitrary permutations of the sequence ordering [20, 42]. We will now demonstrate that under a masking noise process, the discrete flow matching objective is equivalent to the any-order autoregressive objective.

Let us consider a sequence  $x_1 = (x_1^1, x_1^2, \dots, x_1^D)$  from our data distribution. In an any-order autoregressive model, we sample a permutation  $\sigma$  of indices  $\{1, 2, \dots, D\}$  and factorize the joint distribution as:

$$p_\theta(x_1) = \prod_{i=1}^D p_\theta(x_1^{\sigma(i)} | x_1^{\sigma(<i)}) \quad (17)$$

where  $x_1^{\sigma(<i)}$  denotes  $(x_1^{\sigma(1)}, x_1^{\sigma(2)}, \dots, x_1^{\sigma(i-1)})$ . The AO-ARM objective is to maximize the expected log-likelihood over all possible permutations:

$$\mathcal{L}_{\text{AO-ARM}} = \mathbb{E}_{x_1 \sim p_{\text{data}}(x_1), \sigma \sim \text{Unif}(\text{Perm}(D))} \left[ \sum_{i=1}^D \log p_\theta(x_1^{\sigma(i)} | x_1^{\sigma(<i)}) \right] \quad (18)$$

$$= D \mathbb{E}_{x_1 \sim p_{\text{data}}(x_1), \sigma \sim \text{Unif}(\text{Perm}(D)), i \sim \text{Unif}(\{1, \dots, D\})} \left[ \log p_\theta(x_1^{\sigma(i)} | x_1^{\sigma(<i)}) \right] \quad (19)$$

$$= D \mathbb{E}_{x_1 \sim p_{\text{data}}(x_1), i \sim \text{Unif}(\{1, \dots, D\}), \sigma \sim \text{Unif}(\text{Perm}(D))} \left[ \log p_\theta(x_1^{\sigma(i)} | x_1^{\sigma(<i)}) \right] \quad (20)$$

$$= D \mathbb{E}_{x_1 \sim p_{\text{data}}(x_1), t \sim \text{Unif}([0, 1]), x_t \sim p_{t|1}(x_t | x_1)} \left[ \log p_\theta(x_1 | x_t) \right] \quad (21)$$

$$= D \mathcal{L}_{\text{FM}}, \quad (22)$$

where we go from Equation 20 to Equation 21 by recognizing that randomly picking the number of positions to mask and sampling a random permutation is equivalent to picking a random time and sampling the forward noising process for that time. Thus, we have shown that the any-order autoregressive modeling loss is equivalent, up to a constant, to a masking discrete flow matching loss with a uniform noise schedule.

## Decoding ordering in any-order autoregressive models

While the mathematical equivalence between any-order autoregressive models (AO-ARMs) and discrete flow matching is exact in theory, a practical subtlety arises when implementing AO-ARMs with causal attention mechanisms. In practice, many AO-ARMs, including ProteinMPNN [1], are implemented using standard autoregressive architectures with causal attention masks. When computing the probability  $p_\theta(x_1^i | x_t)$  for a masked position  $i$  given a partially masked sequence  $x_t$ , the model must process the unmasked positions in  $x_t$  in some specific order due to the causal nature of the attention mechanism. Formally, for a position  $i \in M_t$  (the set of masked positions), the probability  $p_\theta(x_1^i | x_t)$  should theoretically be independent of how the unmasked

positions in  $U_t = j : x_t^j \neq ?$  are ordered. However, in practice, the causal attention mechanism means that:

$$p_\theta(x_1^i | x_t) = p_\theta(x_1^i | x_t^{\sigma(1)}, x_t^{\sigma(2)}, \dots, x_t^{\sigma(|U_t|)}) \quad (23)$$

where  $\sigma$  is some permutation of the unmasked positions in  $U_t$ , and the probability depends on this specific ordering  $\sigma$ . During training, the any-order autoregressive objective encourages the model to produce consistent predictions regardless of the permutation  $\sigma$ . The expectation over all possible permutations in the training objective should, in principle, ensure that  $p_\theta(x_1^i | x_t)$  is invariant to the ordering of unmasked positions. However, in practice, this invariance may not be perfectly achieved due to imperfect optimization and finite-sample training. To address this subtlety and ensure consistent behavior during guided sampling, for the protein stability experiment that guides ProteinMPNN, we fix the decoding ordering for  $x_t$  based on the residue positions of the unmasked tokens. Specifically, we sort the unmasked positions in  $U_t$  in ascending order of their sequence positions:

$$\sigma(j) = \text{sort}(U_t)[j] \quad (24)$$

where  $\text{sort}(U_t)$  returns the unmasked positions ordered by their indices in the original sequence. This approach provides a deterministic and reproducible ordering for any given masked state  $x_t$ , respects the natural left-to-right order of residues in the protein sequence, and requires no additional hyperparameters or complex ordering strategies. By using this fixed position-based ordering, we ensure that the conditional probabilities  $p_\theta(x_1^i | x_t)$  are well-defined and consistent across different sampling runs, enabling reliable application of the guidance method to AO-ARM models trained with causal attention.

### Relationship to autoregressive models and discrete time diffusion models on discrete state-spaces

Autoregressive (AR) models represent another important class of generative models for discrete state-spaces that can be connected to the diffusion framework. AR models factorize the joint distribution sequentially as  $p(x_1) = \prod_{i=1}^D p(x_1^i | x_1^1, x_1^2, \dots, x_1^{i-1})$ , generating tokens one at a time in a fixed order. Austin et al. [19] showed that AR models can be interpreted as discrete space diffusion models with a particular form of noising process. For AR models, Yang and Klein [24] introduced FUDGE, a method that performs guidance by modulating each conditional distribution using a learned classifier evaluated on the partially completed sequence. FUDGE can be viewed as a special case of ProteinGuide when applied specifically to AR models.

While discrete time diffusion models [19] are trained with a different objective than their continuous-time counterparts, they can still benefit from our guidance methodology. The learned denoising model from a discrete-time training objective can be used to induce a rate matrix for sampling by assuming smooth interpolation between discrete time points. However, both theoretical analysis and empirical results [31, 33, 37, 38]

suggest that models trained with continuous-time objectives often achieve superior performance in practice.

This relationship between different model classes highlights the generality of ProteinGuide as a framework that can accommodate various generative architectures, including AR models, discrete-time diffusion models in discrete state-spaces, and the continuous-time formulations we primarily focus on in this work.

## Background on diffusion guidance

Guidance is a useful technique that enables conditional generation with diffusion and flow models [13–15]. Originally developed for continuous state-space models, guidance allows steering the generative process toward samples with desired properties without requiring conditional training. In continuous state-space diffusion models, the generation process involves sampling from a reverse stochastic differential equation (SDE) that gradually transforms noise into data [15]. To condition this process on a desired property  $y$ , it has been shown that one can leverage Bayes’ theorem to obtain the conditional score function [15]:

$$\nabla_{x_t} \log p_t(x_t|y) = \nabla_{x_t} \log p_t(x_t) + \nabla_{x_t} \log p_t(y|x_t) \quad (25)$$

This formulation, termed *classifier guidance*, combines the unconditional score  $\nabla_{x_t} \log p_t(x_t)$  with the gradient of a predictor model  $\nabla_{x_t} \log p_t(y|x_t)$ . The strength of guidance can be controlled by introducing a *guidance strength* parameter  $\gamma$  [14]:

$$\nabla_{x_t} \log p_t^{(\gamma)}(x_t|y) = \nabla_{x_t} \log p_t(x_t) + \gamma \nabla_{x_t} \log p_t(y|x_t) \quad (26)$$

This approach provides several advantages: (i) it enables conditioning an unconditional model without retraining, (ii) the guidance strength  $\gamma$  can be adjusted at inference time, and (iii) it allows composition of multiple guidance signals. Ho and Salimans [45] later introduced *classifier-free guidance*, which achieves similar results without an explicit classifier by combining a conditionally trained model and an unconditional model, which in practice are typically trained jointly. Classifier-free guidance has been shown to improve sample quality [45] compared to using only the conditionally trained model, and recent work on *autoguidance* showed further improved sample quality by combining a trained model with a more inferior version of itself [46].

While guidance, either classifier-based, classifier-free or autoguidance, has proven extremely valuable for continuous state-space models, extending these concepts to discrete state-spaces poses unique challenges, since the score functions are not defined and these formulations cannot be directly applied. One can sidestep the need for a score function by instead returning to Bayes’ theorem, which, in the context of diffusion on discrete state-spaces, dictates that we must effectively compute

$$p(x_{t+dt}|x_t, y) = \frac{p(y|x_{t+dt}, x_t)p(x_{t+dt}|x_t)}{\sum_{x'_{t+dt}} p(y|x'_{t+dt}, x_t)p(x'_{t+dt}|x_t)}, \quad (27)$$

where  $x_{t+dt}$  and  $x_t$  are separated by a infinitesimal time step  $dt$ , and  $y$  is the desired property we wish to condition on. In a  $D$ -dimensional discrete state-space where each dimension has cardinality  $S$ , there are  $S^D$  terms in the normalizing constant of Equation 27, rendering it generally intractable. Each term arises from the fact that, without constraints, any state can be reached from any other state. Intuitively, tractability can only be achieved if the number of terms is not exponential, thereby implying some constraints on the allowed state transitions. Next, we shall see how the continuous-time formulation of discrete state-space diffusion and flow models enables us to tractably compute the normalizing constant by imposing such constraints, without losing any model expressibility.

## Guidance in discrete state-spaces

Here we provide a brief overview of the results presented in Nisonoff et al. [16]. To enable guidance for discrete state-space models, we turn to continuous-time diffusion models and flow models in discrete state-spaces. As described above, these models are based on continuous-time Markov chains (CTMCs) and therefore parameterize transition rates  $R_t(x, \tilde{x})$  rather than score functions. These models also assume that the noising processes in each dimension are independent of one another (but not necessarily identical), which has the important consequence that the probability that two or more dimensions of the current state jump (transition) at exactly the same time is zero, which makes these models tractable [31, 37]. It turns out that the same assumption also makes guidance tractable for these models [16].

To perform predictor guidance in this setting, we derived a principled approach to adjust these rates based on a predictor model  $p(y|x_t)$  that evaluates how likely a state  $x_t$  is to have the desired property  $y$  [16]. Specifically, we showed that the conditional rates can be obtained as:

$$R_t(x, \tilde{x}|y) = \frac{p(y|\tilde{x}, t)}{p(y|x, t)} R_t(x, \tilde{x}) \quad (28)$$

for any state  $\tilde{x}$  that differs from  $x$  in at most one dimension. This formulation directly implements Bayes' theorem at the level of transition rates, modulating transitions toward states that have higher likelihood of possessing the desired property.

Similar to continuous state-space guidance, we can control the strength of guidance with a guidance strength parameter  $\gamma$ :

$$R_t^{(\gamma)}(x, \tilde{x}|y) = \left[ \frac{p(y|\tilde{x}, t)}{p(y|x, t)} \right]^\gamma R_t(x, \tilde{x}) \quad (29)$$

or derive predictor-free guidance discrete state-spaces:

$$R_t^{(\gamma)}(x, \tilde{x}|y) = R_t(x, \tilde{x}|y)^\gamma R_t(x, \tilde{x})^{1-\gamma} \quad (30)$$

For computational efficiency, especially with large state-spaces, we introduced Taylor-approximated guidance (TAG) [16], which approximates the likelihood ratio

using a first-order Taylor expansion inspired by Grathwohl et al. [47]:

$$\log \frac{p_\phi(y|\tilde{x}, t)}{p_\phi(y|x, t)} \approx (\tilde{x} - x)^T \nabla_x \log p_\phi(y|x, t) \quad (31)$$

requiring only one forward and one backward pass of the predictor model instead of  $D \times (S - 1) + 1$  forward passes, making estimation of the guide-adjusted rates  $O(1)$  rather than  $O(D \times S)$ . With multiple particles, TAG can be further improved by acting as a proposal distribution in a Sequential Monte Carlo (SMC) algorithm similar to Wu et al. [48]. While there are other recently proposed approaches for guiding discrete diffusion models [49–51], ProteinGuide has the benefit of being both exact and general, applicable to both diffusion and flow-based models, making it a general and flexible framework for guiding a broad class of discrete state-space generative models.

### Additional discussion of related work

Several recent works have proposed related but different techniques from Nisonoff et al. [16] for steering discrete state-space diffusion models. These approaches can be broadly categorized into guidance-based methods (which modify the sampling process at inference time) and fine-tuning approaches (which update the parameters of the pre-trained model).

Li et al. [49] proposed a derivative-free sampling technique for reward maximization in both continuous and discrete spaces using Sequential Monte Carlo (SMC). Their approach uses the unconditional model as the proposal distribution and reweights multiple particles with the reward function. Singhal et al. [51] built upon and generalized the methods in Wu et al. [48] and Li et al. [49] to enable more flexible choices over the sampling hyperparameters. Schiff et al. [50] presented a discrete-time analog of the continuous-time guidance method in Nisonoff et al. [16]. As noted in Schiff et al. [50], in discrete time, the normalizing constant in Equation 27 is still intractable, necessitating additional assumptions to achieve tractability, whereas Nisonoff et al. [16] showed that the continuous-time formulation of discrete diffusion models provides exactly the tractability necessary to perform exact guidance. In addition, the continuous-time formulation naturally enables guidance for discrete state-space flow matching models, whereas the discrete-time formation does not. Lee et al. [52] observed that when applying stronger guidance, sampling can be improved with SMC, aligning with challenges in low-temperature sampling noted in Du et al. [53] and Ingraham et al. [3]. For AR models, Zhao et al. [54] proposed an SMC-based steering method that learns intermediate twist functions via contrastive learning, similar to learning time-dependent predictors in diffusion guidance.

Recent works have also explored updating model parameters to incorporate conditioning rather than modifying the sampling process. Wang et al. [55] proposed to use the Gumbel-Softmax trick to make discrete diffusion trajectories differentiable and enable backpropagation of rewards through entire sampling paths. Concurrently, Rector-Brooks et al. [56] proposed to frame the steering problem as sampling from a Bayesian posterior where the pre-trained model serves as the prior and the reward

acts as the likelihood. Both fine-tuning approaches established connections to Nisonoff et al. [16] while offering complementary perspectives on solving the steering problem.

Direct Preference Optimization (DPO [57]) and related work [11, 58] enable updating of pre-trained models, although up until recently, these methods have been applicable only to models with tractable likelihoods, thereby restricting them largely to autoregressive models. For example, Widatalla et al. [11] applied DPO to ESM-IF1, an autoregressive inverse folding model, to incorporate experimental stability data. In another example, Stocco et al. [59] applied DPO to an autoregressive model conditionally trained on enzyme classes to guide the generation towards various enzyme properties. Wallace et al. [60] extended DPO to diffusion models on continuous state-spaces by way of approximation, while Borso et al. [61] explored how to similarly do so for these models on discrete state-spaces. Importantly, the connections previously mentioned between MLMs, diffusion and flow matching models on discrete state-spaces, and any-order autoregressive models, means that we can also generalize the aforementioned approximate DPO to these same model classes. Herein, we focus our study on plug-and-play guidance, rather than DPO-style approaches, although the latter could prove equally useful. Recent work by Yang et al. [62] compared various guidance-based and fine-tuning based approaches on several in-silico tasks for protein fitness optimization and found guidance-based approaches for discrete state-space diffusion models to be generally more effective than fine-tuning based approaches. In addition, they found that guidance-based approaches require less hyper-parameter tuning and have lower computational costs, making them more practically accessible to everyday users.

Reinforcement Learning from Human Feedback (RLHF) offers an alternative approach to model alignment through methods like Proximal Policy Optimization (PPO) [63]. PPO does not technically require the retrained model to have tractable likelihoods, but it requires an explicit reward model and on-policy training, making it often more complicated to train than more direct approaches like DPO [57]. In addition, the standard RLHF pipeline typically begins with more heuristic methods such as continuing to train an existing model with new data (*i.e.*, supervised fine-tuning), for which the statistical outcome is not well-defined, and for which important information from the already-trained model may be forgotten. Blalock et al. [64] recently applied PPO to align protein language models *e.g.*, ESM2 with experimental measurements. Notably, this approach does not directly sample from generative models in the conventional sense; instead, it employs a position-wise scoring strategy where models evaluate mutation probabilities at individual positions sequentially, followed by an iterative selection process that combines high-scoring mutations.

There is another line of work that model discrete data by embedding the data into continuous state-spaces, either on a probabilistic simplex [65] or on a continuous latent space [66, 67]. Some of the approaches proposed to apply guidance to diffusion models on the continuous state-space representations of discrete state-space objects in order to utilize the guidance approaches for continuous state-space diffusion. For example, Gruver et al. [68] propose to perform guidance in the hidden layers of the unconditional diffusion model by jointly training the unconditional denoising model and the classifier on one hidden layer of the denoising model. In another example, Lisanza et al. [69] propose to fine-tune RoseTTAFold with gaussian diffusion on the

one-hot encoded sequence space in order to perform guidance in this continuous state-space. We note that approaches which perform guidance in continuous spaces lose the discrete structure of the data during generation, which can be important for settings where the discrete structures contain information that are useful for guidance [37].

# Simplified and faster sampling for flow matching and diffusion models with masked noise processes

## Intuitive overview

In previous sections, we showed an equivalence between the loss functions used to train discrete flow-matching models (DFMs), discrete diffusion models (DDM), any-order autoregressive models (AO-ARMs) and masked language models (MLMs), specifically when the DFMs and DDMs used a masked noise process. In this section, we show a relationship between sampling algorithms used for these models. In particular, we show that instead of sampling from a CTMC—the required operation for sampling from a CTMC-based DFM—by way of integration in time using algorithms such as Euler, Gillespie, or Tau-Leaping (of which only Gillespie is exact), that one can instead use a much simpler algorithm to exactly sample from the CTMC. Specifically, one can use a simpler sampling algorithm that is normally used to sample from an AO-ARM.

In particular, we will be able to exactly sample from a CTMC underlying a DFM by independently sampling all transition times up-front—meaning before any state transitions have been sampled—and only then sampling all the state transitions. This lies in stark contrast to general CTMC sampling in which sampling time and state transitions must be interleaved. However, it is exactly how one would sample from an AO-ARM, where one first samples a “decoding order”, and then autoregressively unmask each position in turn according to this order, consider all previously unmasked positions. Consequently, there is a constructive proof below for which AO-ARM to sample from so as to sample from the desired CTMC associated with a DFM. As a corollary, we also show that one only needs the *ordering* of the transition times to sample the state transitions.

In order to achieve correctness of this simplified sampling algorithm, we will need to make use of commonly used modeling choices made for CTMC-based DFMs, such as that these CTMCs follow an interpolation schedule as prescribed by the flow matching set-up. These choices enable us to derive a joint probability distribution for the CTMC over time and sequences that factorizes in the necessary way, namely into a term containing solely transition (holding) times, and another containing solely state transitions.

So far we have discussed only DFMs, but through other work that connects DFMs as a generalization of DDMs (see 5), these diffusion models inherit all the work of sampling from a DFM. We will discuss related work for DFMs below.

In addition to showing simplified and faster sampling for CTMC-based DFMs, we also, to the best of our knowledge, show for the first time how to use this new viewpoint to provide an alternative derivation for the guidance results for CTMC-based diffusion and flow matching models presented in Nisonoff et al. [16].

Because we showed earlier that the training objective for MLMs is the same as for AO-ARM and MDMs, we can similarly appeal to our earlier reasoning of interpreting an MLM as either an AO-ARM or DFM, and correspondingly also sample from it in the same as described herein.

## Related work

A number of existing works have discussed the topics herein, but these works are for the specific case of diffusion models, namely CTMC-based MDMs. We prove similar results for the case of flow matching models, namely CMTC-based MFMs. We also synthesize these results from prior work to give a coherent, constructive proof for the equivalence of paths sampled by MFMs and AO-ARM.

As mentioned above, it has been previously shown that sampling exactly from the CTMC of a MDM is equivalent to sampling unmasking times for each position upfront and then using this to define the decoding order to sample from an AO-ARM [20–22, 39, 70–72]. The discussions in Ou et al. [72] and Peng et al. [39] are most similar to this section in spirit, but again, analyze the equivalence for MDMs specifically. Furthermore, neither works give a unified proof of the equivalence in sampling which allows complete removal of the notion of time when sampling from an MFM, showing equivalence for the full path and not just marginal distributions. Appendix H of Campbell et al. [37] further shows a correspondence between DDMs and DFMs where DFMs define a large class of rate matrices for which DDMs correspond to a specific choice. We believe this holds in the general case, such that our results for MFMs should be reducible to the previously cited results for MDMs.

Previous works by Campbell et al. [37], Gat et al. [38] on MFMs have mentioned that the conditional distribution parameterized by the neural network is independent of time (see [21, 22, 39] for the analogous MDM results). This is a key insight that we use in this section as well. However, as used by prior work, we do not believe this insight suffices to show the AO-AR sampling method for MDMs samples the desired CTMC, nor does it directly extend the MDM proofs to MFMs. Herein, we provide a proof of the exact equivalence, which additionally gives a method to sample the transition times. Integrating these findings, Proposition 1 gives us a constructive proof to sample from the desired CTMC using either an MFM or an AO-ARM.

Our proofs hold for the common MFM formulation from Campbell et al. [37], Gat et al. [38], which we define again in 5. Many of the results can readily be extended to other noise distributions, such as uniform substitutions, or to the use of stochasticity and corrector sampling. However, in those cases, a full reduction to AO-ARM sampling is not possible. Instead, the calculations yield an efficient Gillespie sampling algorithm, which we do not cover in detail.

## Background and notation for AO-ARMs, CTMCs, and DFMs

In this section, we briefly review the relevant concepts for AO-ARMs, CTMCs, and flow-matching models. Although some of these were covered earlier, here we quickly remind the reader so as to also introduce notation convenient specifically to this section.

### Any-order autoregressive models (AO-ARMs)

Sampling from an AO-ARM [20, 42, 73, 74] involves iteratively constructing a sample,  $X = (X^1, \dots, X^D)$  of length  $D$ , starting from a fully masked sequence, in two steps. First, a permutation,  $\sigma$ , of positions,  $1, 2, \dots, D$  is sampled uniformly at random. This

permutation dictates the order of positions to unmask as the sample is constructed over  $D$  iterations (one for each position), sometimes called the “decoding order”. Given the permutation ordering,  $\sigma(1, 2, \dots, D)$ , the model progressively unmasks each position according to this ordering, one at a time, autoregressively. That is, at each step, the model samples from the conditional distribution,  $X^{\sigma(i)} \sim p(X^{\sigma(i)} | x^{\sigma(<i)})$ . These distributions are the core object learned when training an AO-ARM, typically by a neural network. We denote the set of progressively unmasked sequences generated during the autoregressive sampling as  $\mathbf{X} = (X_1, \dots, X_D)$ , where bold indicates a ordered set of random variables, and subscript denotes the  $i^{\text{th}}$  unmasking iteration. Note that both the dimension of  $X$  is  $D$ , and that there are  $D$  unmasking operations to generate it, which can be confusing. We sometimes refer to  $\mathbf{X}$  as the “path”. We can also represent the path compactly as a tuple of the decoding order and the final sequence, denoted  $\mathbf{X} = (\sigma, X)$ .

Formally, we write the joint probability of the permutation ordering,  $\sigma$ , and the fully unmasked sequence,  $X$  (together sometimes called the “decoding path”) as

$$\mathbb{P}_{\text{OA}}(\sigma, X) = U[S_D](\sigma) \prod_{i=1}^D p\left(X^{\sigma(i)} | x^{\sigma(<i)}\right), \quad (32)$$

where  $S_D$  is the group of permutations over sequences of length  $D$ ,  $U[S_D](\sigma)$  indicates  $\sigma$  is sampled uniformly at random from  $S_D$ ,  $X^{\sigma(i)}$  is the random variable for the value of position  $\sigma(i)$ , and  $x^{\sigma(<i)}$  is the set of  $i - 1$  observed positions that are unmasked at the  $i$ -th decoding step.

## Continuous Time Markov Chains (CTMCs)

Continuous time Markov chains (CTMCs) describe a sequence of Markovian transitions between discrete states as a continuous time process. For a detailed introduction, including path probability calculations like the ones done here, see Del Moral and Penev [75]. When a CTMC “jumps” from a state  $x$  to state  $\tilde{x}$  at time  $\tau$ , we say that the CTMC experienced a state transition from  $x$  to  $\tilde{x}$  at jump time  $\tau$ . Since the transition is instantaneous, we define the new state to be the state at time  $\tau$ :  $X_\tau = \tilde{x}$ . Accordingly, we say the previous state  $x$  is the left limit of the CTMC at time  $\tau$ , meaning it is the value of the CTMC going right up to the jump time. We denote the left limit  $X_{\tau_i}^- = \lim_{t \nearrow \tau_i} X_t = X_{\tau_i-1}$ .

We will often omit the random variables when symbol for the observed value is the corresponding lower-case letter. For example,  $\mathbb{P}_{\text{MFM}}(x_t) = \mathbb{P}_{\text{MFM}}(X_t = x_t)$  refers to the probability of observing the random variable  $X_t$  taking on value  $x_t$ . Sometimes, when the variable for the observed value does not correspond to the random variable it is assigned to, we will write both explicitly. For example, in writing  $\mathbb{P}_{\text{MFM}}(x_t | X_t^- = x_s)$  we refer to the probability that the masked flow matching model (MFM) transitions from  $x_s$ , the state it reached at a previous time  $s$ , to  $x_t$  at time  $t$ . Recall that  $X_t^- = x_s$  indicates that the state  $x_s$  is the left limit  $X_t^-$  of the state at  $t$ .

Finally, the rate matrix from  $x$  to  $\tilde{x}$  at time  $t$  is denoted  $R_t(x, \tilde{x})$ . The rate matrix is generally time-dependent even when conditioned on the state. In flow-matching models, transition rates between states generally accelerate in time to ensure the

process terminates by time  $t = 1$ . Accordingly, the CDF of the jump time, is an integral of time-dependent rates and does not always have a closed-form expression. It is written as

$$\mathbb{P}(T_k < t \mid T_{k-1}) = 1 - \exp\left(\int_{s=T_{k-1}}^{s=t} R_s(X_s^-, X_s^-) ds\right). \quad (33)$$

As one can see, this integrates the rate of the CTMC not undergoing a state transition at time  $s$ .

### Discrete flow-matching models (DFMs)

Discrete flow matching models (DFMs) were formulated by Campbell et al. [37], Gat et al. [38] to define a CTMC whose marginal distribution over states interpolates between a noise distribution  $p_{\text{noise}}$  at time 0 and a data distribution  $p_{\text{data}}$  at time 1.

Formally, this requires that the rates learned by our DFMs are solutions to the Kolmogorov Forward Equation (KFE) that satisfy the interpolation  $X_t = \kappa_t X_1 + (1 - \kappa_t) X_0$  subject to  $X_1 \sim p_{\text{data}}$  and  $X_0 \sim p_{\text{noise}}$ . The *interpolation schedule*  $\kappa_t$  sets the probability of finding  $X_t$  in the denoised state  $X_1$  at each time  $t$ . The interpolation schedule can be freely defined by the user so long as  $\kappa_0 = 0$  and it monotonically increases to  $\kappa_1 = 1$ . Note, for the MFMs analyzed in this section, this means we can interpret  $\kappa_t$  is the CDF of the jump time for a position,  $\kappa_t = \mathbb{P}(\tau < t)$ . This, in turn, implies that the time derivative is the PDF of the jump time,  $\dot{\kappa}_t = \mathbb{P}(\tau = t)$ .

The CTMC underlying a DFM is used to sample transport paths to map samples from  $p_{\text{noise}}$  to final samples from  $p_{\text{data}}$ , the distribution the DFM seeks to model. The transport is simulated by sampling a sequence  $X_0 \sim p_{\text{noise}}$  (all masked in the case of a masked flow-matching model, MFM) and numerically integrating the CTMC by sampling

$$X_{t+\Delta t} \sim p_{t+dt|dt}(\cdot|x_t) \approx \delta_{x_t}(\cdot) + R(x_t, \cdot)\Delta t$$

until we reach  $X_1 \sim p_{\text{data}}$ .

The formulation of DFMs from Campbell et al. [37], Gat et al. [38] which was described above, makes three important assumptions:

1. the conditional rates of the CTMC factorize per position, when conditioned on the denoised sequence  $X_1$ ,
2. the rates of multiple positions changing in the CTMC simultaneously is 0,
3. the interpolation schedule  $\kappa_t$  is independent of the partially denoised sequence  $X_t$ .

Given these conditions for the DFM, the rates for each position  $i$  can be found analytically to be

$$R_t^i(x_t^i, \tilde{x}) = \frac{\dot{\kappa}_t}{1 - \kappa_t} (p_{1|t}(X_1^i = \tilde{x} | X_t = x_t) - \delta_{x_t^i}(\tilde{x}^i)), \quad (34)$$

where  $p_{1|t}(X_1^i = \tilde{x} | X_t = x_t) - \delta_{x_t^i}(\tilde{x}^i)$  is the key object learned by a machine learning model. Note that this expression for the rates factors into two terms. The first is the probability of a transition occurring at time  $t$ ,  $\mathbb{P}_{\text{MFM}}(\tau = t | \tau \geq t) = \frac{\dot{\kappa}_t}{1 - \kappa_t}$ . The second,

$p_{1|t}(X_1^i = \tilde{x}|X_t = x_t) - \delta_{x_t^i}(\tilde{x}^i)$ , ensures that if there is a jump (when  $\delta_{x_t^i}(\tilde{x}^i) = 0$ ), the state will be sampled from  $p_{1|t}$ . This will be discussed in more detail in the proofs of the lemmas.

Similar to AO-ARMs, where we represent the sequence of partially unmasked states as the tuple  $(\sigma, X)$ , we represent the sequence of transitions in a sampled MFM path as the tuple  $(\boldsymbol{\tau}, \mathbf{X})$ . Here,  $\boldsymbol{\tau} = (\tau_0 = 0, \tau_1, \dots, \tau_D < 1)$  is the sequence of transition times sampled by the CTMC, in increasing order, from 0 to 1. As before,  $\mathbf{X} = (X_0, X_{\tau_1}, \dots, X_{\tau_D})$  is the sequence of states at each of those times. Note that  $X_0$  is the all masked state and the fully unmasked state is  $X_1 = X_D$ .

As in the AO-ARM case, we say that  $\sigma$  is the permutation that maps from transition times to the position of the sequence that changed. Concretely, the  $i$ -th transition occurs at time  $\tau_i$  and causes the  $\sigma(i)$ -th position to be unmasked. Like AO-ARMs, this means we can also represent  $\mathbf{X}$  as the tuple  $(\sigma, X_{\tau_D})$ . We can also use  $\sigma$  to sort the transition times of each position  $\mathbf{T} = (T_1, \dots, T_D)$  into the transition times of the CTMC:  $\sigma(\mathbf{T}) = \boldsymbol{\tau}$ .

Below, we have included an expression for the probability of a CTMC path sampled using an MFM. This particular formula applies to all CTMCs and does not readily admit an algorithmic implementation, we just include it here for completeness:

$$\begin{aligned} & \mathbb{P}_{\text{MFM}}(\boldsymbol{\tau}, \mathbf{X}) \\ &= \mathbb{P}_{\text{MFM}}(\tau_0, x_{\tau_0}) \times \prod_{i=1}^D \mathbb{P}_{\text{MFM}}(\tau_i, x_{\tau_i} | \tau_{i-1}, x_{\tau_{i-1}}) \times \mathbb{P}_{\text{MFM}}(\tau_{D+1} > 1 | \tau_D, x_{\tau_D}). \end{aligned}$$

### MFM CTMCs use the minimal number of transitions

Campbell et al. [37], Gat et al. [38] shows that the rates defined above (Eq. 34) make the minimal number of jumps needed to denoise the sequence. In the case of an MFM, this means we have exactly  $D$  transitions, one to unmask each position. However, there is an infinite class of rate matrices which also solve the KFE and DFM boundary conditions, which do not have this minimal jumps property.

Non-minimal rate matrices can be formulated as those with non-zero stochasticity as in Campbell et al. [37], and can be equivalently formulated through corrector sampling Gat et al. [38]. Our proofs explicitly handle the minimal case, but the calculations can be readily extended to the case of non-zero stochasticity. We do note, however, that when doing *exact* sampling, rate matrices with non-zero stochasticity yield the same time-marginals as the minimal rates (by construction). Generally, non-zero stochasticity is only useful when  $\Delta t$  is large enough during numerical integration that multiple positions are sampled at once. In such settings, stochasticity is believed to correspond to implicit “equilibration” steps that reduce drift in the simulated CTMC.

### Statement and proof of exact MFM sampling using AO-ARMs

We show that paths from a masked flow matching model’s (MFM’s) CTMC can be sampled *exactly* by sampling transition times uniformly at random and sampling state transitions from an AO-ARM independently. The key fact underlying our proof of

Prop. 1 is that the transition times and states for an MFM are conditionally independent of each other given a decoding order. In particular, the distribution over paths factorizes into two terms. The jump time component reduces to a product of  $D$  independent uniform distributions, one for each position; the state transition component yields a product of denoising terms that correspond to the conditional distributions sampled by an AO-ARM. These preceding two statements are proved in Lemmas 1 and 2, respectively, in section 5. Finally, Cor. 1 extends the claim of 1 to shows how to construct a sampler where the decoding order is sampled upfront and the transition times and states are truly sampled independently.

**Proposition 1** *The probability of sampling a path  $(\boldsymbol{\tau}, \mathbf{X})$  from an MFM is equivalent to the probability of*

1. *sampling transition times for each position in the sequence  $\mathbf{T} = (T^1, \dots, T^D)$ , uniformly at random (u.a.r), from the interval  $[0,1]$ ,*
2. *sorting  $\mathbf{T}$  in increasing order to obtain a permutation  $\sigma$ , which maps the unmasking order to the unmasked position,*
3. *setting  $\boldsymbol{\tau} = \sigma(\mathbf{T})$ , where  $\sigma$  acts as  $\tau_i = T^{\sigma(i)}$*
4. *sampling the sequence of states  $\mathbf{X}$  from a AO-ARM using order  $\sigma$  with the conditional distribution for predicting the next position set to the MFM probability denoiser:  $p(X^{\sigma(i)} = \tilde{x} | X^{\sigma(<i)} = x) := p_{1|t}(X_1 = \tilde{x} | X_t^- = x)$ .*

Below,  $\mathbb{P}_{\text{OA}}$  refers to the distribution induced by the resulting AO-ARM in point (4) above. We call this resultant model the “equivalent” AO-ARM for our MFM. Note that we can also obtain the equivalent MFM for an AO-ARM by reversing the assignment of conditional distributions.

Altogether, these four points correspond to following equation:

$$\mathbb{P}_{\text{MFM}}(\boldsymbol{\tau}, \mathbf{X} = (\sigma, X_{\tau_D})) = U_{[0,1]}^D(\mathbf{T} = \sigma^{-1}(\boldsymbol{\tau})) \mathbb{P}_{\text{OA}}(X = X_{\tau_D} | \sigma),$$

where  $\sigma^{-1}$  acts as  $T^j = \tau_{\sigma^{-1}(j)}$  and  $U_{[0,1]}^D$  is the product of  $D$  independent uniform distributions on the interval  $[0, 1]$ .

We use this notation to show that the density of sampling  $\boldsymbol{\tau}$  and  $\mathbf{X}$  from an MFM is the same as the probability of (1) sampling  $\mathbf{T}$  u.a.r, inducing a associated decoding order  $\sigma$  and  $\boldsymbol{\tau}$  as a result, and (2) using that decoding order to recover  $\mathbf{X}$  from an AO-ARM, as described at the beginning of the proposition.

*Proof* Since CTMCs are, by definition memoryless (depend only on the previous time and state), the path probability density decomposes into a product of densities for each transition conditioned on the last. This can be written as

$$\begin{aligned} & \mathbb{P}_{\text{MFM}}(\boldsymbol{\tau}, \mathbf{X}) \\ &= \mathbb{P}_{\text{MFM}}(\tau_0, x_{\tau_0}) \times \prod_{i=1}^D \mathbb{P}_{\text{MFM}}(\tau_i, x_{\tau_i} | \tau_{i-1}, x_{\tau_{i-1}}) \times \mathbb{P}_{\text{MFM}}(\tau_{D+1} > 1 | \tau_D, x_{\tau_D}). \end{aligned}$$

The MFM always starts at time  $\tau_0 = 0$  with the fully masked sequence  $x_0 = \{M\}^D$  so  $\mathbb{P}_{\text{MFM}}(\tau_0, x_{\tau_0}) = 1$ . There are also exactly  $D$  transitions because we assume 0 stochasticity and no corrector sampling. This means  $\mathbb{P}_{\text{MFM}}(\tau_{D+1} > 1 | \tau_D, x_{\tau_D}) = 1$  as well. The above now simplifies to

$$\begin{aligned} &= \prod_{i=1}^D \mathbb{P}_{\text{MFM}}(\tau_i, x_{\tau_i} | \tau_{i-1}, x_{\tau_{i-1}}) \\ &= \prod_{i=1}^D \mathbb{P}_{\text{MFM}}(\tau_i | \tau_{i-1}, x_{\tau_{i-1}}) \mathbb{P}_{\text{MFM}}(x_{\tau_i} | \tau_i, x_{\tau_{i-1}}). \end{aligned}$$

We can apply Lemma 1 to remove the state dependence from the conditional distribution over jump times,  $\mathbb{P}_{\text{MFM}}(\tau_i | \tau_{i-1}, x_{\tau_{i-1}})$ . Similarly, we can apply Lemma 2 to remove the time dependence from the conditional distribution over jump states,  $\mathbb{P}_{\text{MFM}}(x_{\tau_i} | \tau_i, x_{\tau_{i-1}})$ . This is the key step of the proof, allowing us to separate the time- and state-dependent distributions into separate terms as follows

$$\begin{aligned} &= \prod_{i=1}^D \mathbb{P}_{\text{MFM}}(\tau_i | \tau_{i-1}) \mathbb{P}_{\text{MFM}}(x_{\tau_i} | x_{\tau_{i-1}}) \\ &= \left( \prod_{i=1}^D \mathbb{P}_{\text{MFM}}(\tau_i | \tau_{i-1}) \right) \left( \prod_{i=1}^D \mathbb{P}_{\text{MFM}}(x_{\tau_i} | x_{\tau_{i-1}}) \right). \end{aligned}$$

In Lemmas 1 and 2 we also calculate closed-form expressions for  $\mathbb{P}_{\text{MFM}}(\tau_i | \tau_{i-1})$  and  $\mathbb{P}_{\text{MFM}}(x_{\tau_i} | x_{\tau_{i-1}})$ , which can be substituted in and simplified as follows

$$= \prod_{i=1}^D \dot{\kappa}_{\tau_i} \times \prod_{i=1}^D p_{1|\tau_i}(X_1 = x_{\tau_i} | X_{\tau_i}^- = x_{\tau_{i-1}}).$$

Now, we will rewrite these products to directly match the proposition statement. First, the interpolation schedule  $\kappa_t$  is the CDF of the jump time under the assumption of minimal transitions. This means the PDF of the jump time for a given position is  $\mathbb{P}_{\text{MFM}}(\tau = t) = \frac{d}{dt} \mathbb{P}_{\text{MFM}}(\tau < t) = \dot{\kappa}_t$ . Generally, we choose  $\kappa_t = t$  so the PDF of the jump times is uniform  $\mathbb{P}_{\text{MFM}}(t = \tau) = \dot{\kappa}_t = 1 = U_{[0,1]}(t = \tau)$ :

$$= \prod_{i=1}^D U[0, 1](\tau_i) \times \prod_{i=1}^D p_{1|\tau_i}(X_1 = x_{\tau_i} | X_{\tau_i}^- = x_{\tau_{i-1}}).$$

Finally, we recognize that the AO-ARM constructed for the sampling algorithm uses the MFM denoiser as its conditional distribution. This means the second product above is just the conditional probability of the sample under the AO-ARM and the expression simplifies to

$$\begin{aligned} &= \prod_{i=1}^D U[0, 1](\tau_i) \times \prod_{i=1}^D p(X^{\sigma(i)} = x_{\tau_i} | X^{\sigma(<i)} = x_{\tau_{i-1}}) \\ &= U^D[0, 1](\mathbf{T} = \sigma^{-1}(\boldsymbol{\tau})) \times \mathbb{P}_{\text{OA}}(X = X_{\tau_D} | \sigma) \end{aligned}$$

as claimed.  $\square$

**Corollary 1** *An MFM can be exactly sampled by first sampling a permutation  $\sigma \sim U[S_D]$  and then sampling the sequence of states for each transition from an AO-ARM. The transition times can then be sampled uniformly at random and assigned to positions according to the sampled permutation.*

*Proof* This follows directly from Proposition 1. Originally, we found

$$\mathbb{P}_{\text{MFM}}(\boldsymbol{\tau}, \mathbf{X}) = \mathbb{P}_{\text{OA}}(X_{\tau_D} | \sigma) U^D[0, 1](\mathbf{T} = \sigma^{-1}(\boldsymbol{\tau}))$$

To be able to sample both the times and permutations independently, upfront, our sampler must find the permutation  $\pi$  that maps the sampled transition times  $\mathbf{T}$  to sampled positions. Then applying  $\sigma$  to  $\pi(\mathbf{T})$  sorts the times to be  $\boldsymbol{\tau}$ . In practice, we would just assign the sampled times to positions in the order specified by  $\sigma$ . For the purposes of this proof, however,  $\pi$  lets us rewrite this expression as:

$$= U[S_D](\sigma) \mathbb{P}_{\text{OA}}(X_{\tau_D} | \sigma) U^D[0, 1](\mathbf{T} = \pi^{-1}(\sigma^{-1}(\boldsymbol{\tau})))$$

Finally, we apply the definition of OA-AR sampling

$$= \mathbb{P}_{\text{OA}}(\mathbf{X}) U^D[0, 1](\mathbf{T})$$

□

Together with Prop 1 this completes our claim of conditional independence of the times and states given the unmasking ordering. In Cor. 1 we can see plainly that the density of paths under the MFM CTMC is the same as sampling from the times and states independently once we've sampled the permutation upfront. Furthermore, the corollary shows that to get the likelihood of an output sequence under the CTMC's final distribution, the specific jump times can be marginalized out easily, but the decoding order still makes getting likelihoods intractable.

## Statements and proofs of lemmas

**Lemma 1** *The conditional probability of the next jump time for an MFM depends only on the previous jump time and can be expressed in closed form as:*

$$\begin{aligned} \mathbb{P}_{\text{MFM}}(\tau_i | \tau_{i-1}, x_{\tau_{i-1}}) &= \mathbb{P}_{\text{MFM}}(\tau_i | \tau_{i-1}) \\ &= (D - (i - 1)) \frac{\kappa_{\tau_i}}{1 - \kappa_{\tau_{i-1}}} \left( \frac{1 - \kappa_{\tau_i}}{1 - \kappa_{\tau_{i-1}}} \right)^{D-i}. \end{aligned} \quad (35)$$

This is the probability that any *one* of the remaining  $D - (i - 1)$  masked positions transitions at time  $\tau_i$ ,<sup>4</sup> given that none of them transitioned between  $\tau_{i-1}$  and  $\tau_i$  and all other positions have already been unmasked.

The core insight from the calculation below is that, in a masking process, the time to the next jump only depends on state through the total number of masked tokens: the rate of leaving the mask state is the same across positions, and once unmasked, the state is fixed.<sup>5</sup> As a result, once one specifies that we're sampling the  $i$ -th jump time, *we know exactly how many masked tokens are left* and there is no further dependence on the CTMC state.

*Proof*

We start by rewriting the PDF of the holding time as the derivative of its CDF,

$$\mathbb{P}_{\text{MFM}}(\tau_i | \tau_{i-1}, x_{\tau_{i-1}})$$

---

<sup>4</sup>  $\frac{\kappa_{\tau_i}}{1 - \kappa_{\tau_{i-1}}} = \mathbb{P}_{\text{MFM}}(\tau_i | \tau_i > t)$

<sup>5</sup> Recall, there are exactly  $D$  jumps because we are using the zero-stochasticity rates from [37, 38].

$$= \frac{\partial}{\partial \tau_i} \mathbb{P}_{\text{MFM}} (T_i < \tau_i | \tau_{i-1}, x_{\tau_{i-1}})$$

which, for CTMCs has the standard form

$$= \frac{\partial}{\partial \tau_i} \left( 1 - \exp \left( \int_{\tau_{i-1}}^{\tau_i} R_s(x_{\tau_{i-1}}, x_{\tau_{i-1}}) ds \right) \right).$$

The rates for two positions transitioning at once are zero [37] so we can factor this expression for the sequence not changing into a product of the probabilities for each position not changing.

$$= \frac{\partial}{\partial \tau_i} \left( 1 - \prod_{i=1}^D \exp \left( \int_{\tau_{i-1}}^{\tau_i} R_s^{\sigma(i)}(x_{\tau_{i-1}}, x_{\tau_{i-1}}) ds \right) \right).$$

We can also substitute in the explicit form of the rates (Eq. (34)), taking care that these are the rates for *not* transitioning away from  $x_{\tau_{i-1}}$

$$= \frac{\partial}{\partial \tau_i} \left( 1 - \prod_{i=1}^D \exp \left( \int_{\tau_{i-1}}^{\tau_i} -\frac{\dot{\kappa}_s}{1 - \kappa_s} \left( 1 - p_{1|\tau_i}^\theta (X_1^{\sigma(i)} = x_{\tau_i}^{\sigma(i)} | X_{\tau_i}^- = x_{\tau_{i-1}}) \right) ds \right) \right)$$

Because these MFM only make the minimal number of transitions, if the current state at position  $i$  is unmasked, we know it will not change. Therefore,  $p_{1|t}^\theta(\cdot | X_t \neq M) = \delta_{X_t}(\cdot)$  and we can drop the terms corresponding to the unmasked positions to get

$$= \frac{\partial}{\partial \tau_i} \left( 1 - \prod_{j \in \sigma(\geq i)} \exp \left( \int_{\tau_{i-1}}^{\tau_i} -\frac{\dot{\kappa}_s}{1 - \kappa_s} \left( 1 - p_{1|\tau_i}^\theta (X_1^j = x_{\tau_i}^j | X_{\tau_i}^- = x_{\tau_{i-1}}) \right) ds \right) \right).$$

We can now drop the state dependence entirely by noting that  $p_{1|t}^\theta(M|\cdot) = 0$  because masked tokens are never in the denoised sequence  $X_1$ :

$$= \frac{\partial}{\partial \tau_i} \left( 1 - \prod_{j \in \sigma(\geq i)} \exp \left( \int_{\tau_{i-1}}^{\tau_i} -\frac{\dot{\kappa}_s}{1 - \kappa_s} ds \right) \right).$$

Simplifying, we find

$$\begin{aligned} &= \frac{\partial}{\partial \tau_i} \left( 1 - \prod_{j \in \sigma(\geq i)} \exp \left( \int_{\tau_{i-1}}^{\tau_i} \frac{d}{ds} \ln(1 - \kappa_s) ds \right) \right) \\ &= \frac{\partial}{\partial \tau_i} \left( 1 - \prod_{j \in \sigma(\geq i)} \frac{1 - \kappa_{\tau_i}}{1 - \kappa_{\tau_{i-1}}} \right) \\ &= -\frac{\partial}{\partial \tau_i} \left( \frac{1 - \kappa_{\tau_i}}{1 - \kappa_{\tau_{i-1}}} \right)^{D-(i-1)} \\ &= (D - (i - 1)) \frac{\dot{\kappa}_{\tau_i}}{1 - \kappa_{\tau_{i-1}}} \left( \frac{1 - \kappa_{\tau_i}}{1 - \kappa_{\tau_{i-1}}} \right)^{D-i} \\ &= (D - (i - 1)) P(\tau_i | \tau_i > \tau_{i-1}) \prod_{j \in \sigma(> i)} P(\tau_j > \tau_i | \tau_i > \tau_{i-1}) \end{aligned}$$

as claimed.  $\square$

**Lemma 2** *The distribution over state transitions is independent of the jump time, and can be expressed in closed-form as follows:*

$$\begin{aligned}\mathbb{P}_{\text{MFM}}(x_{\tau_i}|\tau_i, X_{\tau_i}^- = x_{\tau_{i-1}}) &= \mathbb{P}_{\text{MFM}}(x_{\tau_i}|\tau_i, X_{\tau_i}^- = x_{\tau_{i-1}}) \\ &= \frac{p_{1|\tau_i}^\theta(X_1^{\sigma(i)} = x_{\tau_i}^{\sigma(i)}|X_{\tau_i}^- = x_{\tau_{i-1}})}{D - (i - 1)}\end{aligned}\quad (36)$$

Note that the  $t$  in  $p_{1|t}^\theta$  is suggestive but is often not an explicit input to the model. See Shi et al. [21], Sahoo et al. [22], Ou et al. [72] for further discussion of the analogous results and implications of the lemma for MDMs. In particular, Sahoo et al. [22] provide some empirical results showing that inputting time to the model is unnecessary for MDMs.

*Proof* There is a vanishingly small chance that two positions jump at the same time [37]. Accordingly, we first examine only the conditional distribution for the position that changes. We can write it as

$$\begin{aligned}& \mathbb{P}_{\text{MFM}}\left(X_{\tau_i}^{\sigma(i)} = x_{\tau_i}^{\sigma(i)}|\tau_i, X_{\tau_i}^- = x_{\tau_{i-1}}\right) \\ &= \mathbb{P}_{\text{MFM}}\left(X_{\tau_i}^{\sigma(i)} = x_{\tau_i}^{\sigma(i)}|X_{\tau_i}^{\sigma(i)} \neq M, X_{\tau_i}^{\sigma(i)-} = M, X_{\tau_i}^- = x_{\tau_{i-1}}\right) \\ &= \frac{\mathbb{P}_{\text{MFM}}\left(X_{\tau_i}^{\sigma(i)} = x_{\tau_i}^{\sigma(i)}|X_{\tau_i}^- = x_{\tau_{i-1}}\right)}{\mathbb{P}_{\text{MFM}}\left(X_{\tau_i}^{\sigma(i)} \neq M|X_{\tau_i}^- = x_{\tau_{i-1}}\right)} \\ &= \frac{R_t^{\sigma(i)}\left(M, x_{\tau_i}^{\sigma(i)}|X_{\tau_i}^- = x_{\tau_{i-1}}\right) dt}{\sum_{\tilde{x} \neq M} R_t^{\sigma(i)}\left(M, \tilde{x}|X_{\tau_i}^- = x_{\tau_{i-1}}\right) dt} \\ &= \frac{R_t^{\sigma(i)}\left(M, x_{\tau_i}^{\sigma(i)}|X_{\tau_i}^- = x_{\tau_{i-1}}\right)}{-R_t^{\sigma(i)}\left(M, M|X_{\tau_i}^- = x_{\tau_{i-1}}\right)} \\ &= \frac{\frac{\dot{\kappa}_{\tau_i}}{1 - \kappa_{\tau_i}}\left(p_{1|\tau_i}^\theta(X_1^{\sigma(i)} = x_{\tau_i}^{\sigma(i)}|X_{\tau_i}^- = x_{\tau_{i-1}}) - \delta_{x_{\tau_i}^{\sigma(i)}, M}\right)}{-\frac{\dot{\kappa}_{\tau_i}}{1 - \kappa_{\tau_i}}\left(p_{1|\tau_i}^\theta(X_1^{\sigma(i)} = M|X_{\tau_i}^- = x_{\tau_{i-1}}) - \delta_{M, M}\right)}.\end{aligned}$$

Notice that here we lose all time dependency,

$$\begin{aligned}& \frac{p_{1|\tau_i}^\theta(X_1^{\sigma(i)} = x_{\tau_i}^{\sigma(i)}|X_{\tau_i}^- = x_{\tau_{i-1}})}{\delta_{M, M}} \\ &= p_{1|\tau_i}^\theta(X_1^{\sigma(i)} = x_{\tau_i}^{\sigma(i)}|X_{\tau_i}^- = x_{\tau_{i-1}}).\end{aligned}$$

However, we still need to account for the fact that, out of all unmasked positions,  $\sigma(i)$  was the one that changed.

$$\begin{aligned}& \mathbb{P}_{\text{MFM}}(x_{\tau_i}|\tau_i, X_{\tau_i}^- = x_{\tau_{i-1}}) \\ &= p_{1|\tau_i}^\theta(X_1^{\sigma(i)} = x_{\tau_i}^{\sigma(i)}|X_{\tau_i}^- = x_{\tau_{i-1}}) \frac{p_{1|\tau_i}^\theta(X_1^{\sigma(i)} \neq M|X_{\tau_i}^- = x_{\tau_{i-1}})}{\sum_{j \in \sigma(\geq i)} p_{1|\tau_i}^\theta(X_1^{\sigma(i)} \neq M|X_{\tau_i}^- = x_{\tau_{i-1}})}\end{aligned}$$

$$= \frac{p_{1|\tau_i}^\theta(X_1^{\sigma(i)} = x_{\tau_i}^{\sigma(i)} | X_{\tau_i}^- = x_{\tau_{i-1}})}{D - (i - 1)}$$

as claimed.  $\square$

Although we present a proof for the MFM case, the same calculation can be used to see that the general result for the common class of MFMs described in [37, 38] is:

$$\begin{aligned} & \mathbb{P}_{\text{MFM}}(x_{\tau_i}^{\sigma(i)} | \tau_i, X_{\tau_i}^- = x_{\tau_{i-1}}) \\ &= p_{1|\tau_i}^\theta(X_1^{\sigma(i)} = x_{\tau_i}^{\sigma(i)} | X_{\tau_i}^- = x_{\tau_{i-1}}) \frac{1 - p_{1|\tau_i}^\theta(X_1^{\sigma(i)} = x_{\tau_{i-1}}^{\sigma(i)} | X_{\tau_i}^- = x_{\tau_{i-1}})}{D - \sum_{j=1}^D p_{1|\tau_i}^\theta(X_1^{\sigma(j)} = x_{\tau_{i-1}}^{\sigma(j)} | X_{\tau_i}^- = x_{\tau_{i-1}})} \end{aligned}$$

## Implications for guidance

In this section, we will use the equivalence between AO-ARM and MFMs to show a simplified proof of our guidance method in Nisonoff et al. [16]. The calculation done here pertains specifically to MFMs, but can be readily extended to DFMs more broadly. The core underlying intuition is that the jump times and state transitions depend on the current sequence only through  $p_{1|t}^\theta$ . This is because the interpolation schedule is independent of the state. Therefore, when using guidance, only this distribution needs to be modified.

When guiding an MFM, we condition the CTMC such that it samples from  $p_{\text{data}}(x|y)$  instead of  $p_{\text{data}}(x)$ . This corresponds to setting  $\mathbb{P}'_{\text{MFM}}(X_1) = \mathbb{P}_{\text{MFM}}(X_1|y)$  and solving for the appropriate rate matrices  $R'_t$ . Due to Prop. 1, we can instead analyze how to condition the equivalent AO-ARM and then push this change back into our MFM.

*Proof Sketch* The equivalent AO-ARM samples the unmasked values of positions using  $p^\theta(x^{\sigma(i)} | x^{\sigma(<i)}) := p_{1|t}^\theta(X_1^{\sigma(i)} = x^{\sigma(i)} | X_t^- = x^{\sigma(<i)})$ . To condition, we desire to sample from  $p(x^{\sigma(i)} | x^{\sigma(<i)}, y)$  instead. All we require is an expression for this distribution using our existing conditional model, which we get using Bayes rule as follows:

$$\begin{aligned} p^{\theta'}(x^{\sigma(i)} | x^{\sigma(<i)}) &= p^\theta(x^{\sigma(i)} | x^{\sigma(<i)}, y) \\ &= \frac{p(y | x^{\sigma(i)}, x^{\sigma(<i)}) p^\theta(x^{\sigma(i)} | x^{\sigma(<i)})}{p(y | x^{\sigma(<i)})} \\ &= \frac{p(y | x^{\sigma(i)}, x^{\sigma(<i)})}{p(y | x^{\sigma(<i)})} p_{1|t}^\theta(X_1^i = x^{\sigma(i)} | X_t = x^{\sigma(<i)}) \end{aligned}$$

Above,  $p(y | x^{\sigma(i)}, x^{\sigma(<i)})$  is identical to the noisy predictor trained in regular classifier guidance for an MFM. This suffices to recover the exact guidance methodology in Nisonoff et al. [16]. Using the conditioned AO-ARM, we not write the equivalent MFM. There is one subtlety in this translation. Because we are now finding the general form of the rates absent an already sampled set of transition times, and therefore decoding order, we must choose an appropriate order to use the guided AO-ARM's conditional distribution as the guided MFM's probability denoiser.

Say we are looking at the rate for the position  $j$  at a time leading up to the  $i$ -th jump, such that  $\tau_{i-1} < t \leq \tau_i$ . We choose  $\sigma$  such that  $j = \sigma(i)$  and  $\sigma(< i)$  corresponds to the positions currently unmasked in  $x_t$ . With this construction, we find

$$\begin{aligned} R_t^j(x_t^j, \tilde{x}^j) &= \frac{\dot{\kappa}_t}{1 - \kappa_t} \left( p_{1|t}^\theta(X_1^j = \tilde{x}^j | X_t = x_t) - \delta_{x_t^j}(\tilde{x}^j) \right) \\ &= \frac{\dot{\kappa}_t}{1 - \kappa_t} \left( p^\theta(X^{\sigma(i)} = \tilde{x}^j | X^{\sigma(< i)} = x_t) - \delta_{x_t^j}(\tilde{x}^j) \right) \\ &= \frac{\dot{\kappa}_t}{1 - \kappa_t} \left( \frac{p(y | X^{\sigma(i)} = \tilde{x}^j, X^{\sigma(< i)} = x_t)}{p(y | X^{\sigma(< i)} = x_t)} p_{1|t}^\theta(X_1^i = \tilde{x} | X_t = x_t) \right. \\ &\quad \left. - \delta_{x_t^j}(\tilde{x}^j) \right). \end{aligned}$$

In the case that  $x_t^i = \tilde{x}^i$ ,  $\frac{p(y | X_1^i = \tilde{x}, X_t = x_t)}{p(y | X_t = x_t)}$  simplifies to 1, and we can factor out the added ratio of conditional probabilities to get

$$\begin{aligned} &= \frac{\dot{\kappa}_t}{1 - \kappa_t} \frac{p(y | X^{\sigma(i)} = \tilde{x}^j, X^{\sigma(< i)} = x_t)}{p(y | X^{\sigma(< i)} = x_t)} \\ &\quad \times \left( p_{1|t}^\theta(X_1^i = \tilde{x} | X_t = x_t) - \delta_{x_t^j}(\tilde{x}^j) \right). \end{aligned}$$

Altogether, we have

$$R_t^j(x_t^j, \tilde{x}^j) = R_t^j(x_t^j, \tilde{x}^j | y) = \frac{p(y | X^{\sigma(i)} = \tilde{x}^j, X^{\sigma(< i)} = x_t)}{p(y | X^{\sigma(< i)} = x_t)} R_t^j(x_t^j, \tilde{x}^j).$$

□

This result is exactly the one derived in Nisonoff et al. [16] and has two important properties we'd like to point out here.

First, this conditional rate is zero for any transition involving the change of two or more positions, just like the unconditional rates. Therefore, exactly  $D \times (S - 1) + 1$  rates need to be computed, where  $D$  is the number of positions,  $S$  is the size of the alphabet,  $D \times (S - 1)$  are all the 1-Hamming distance jumps for each position in the sequence, and the extra “+1” at the end comes from the rate of the CTMC staying at the current state.

Second, this shows that we can sample from the guided AO-ARM to get exact predictor guidance, and therefore only need to evaluate the classifier  $S$  times: once for each of the possible transitions at the position being decoded. When  $S$  is small enough, this lets us sidestep the need for the Taylor-approximate guidance, which was derived by Nisonoff et al. [16]. They developed TAG due to the intractability of evaluating a classifier  $D \times (S - 1) + 1$  times to run exact guidance when sampling by numerical integration. Using AO-ARM sampling, we show exact guidance can be done with only a constant dependence in the dimension and linear dependence in the alphabet size. Therefore, running TAG with the AO-ARM sampling approach only adds a constant time cost for using guidance.

## Stability-guided inverse folding

We demonstrated how assay-labeled experimental data could be used to condition generative models for protein sequences, improving the success rates for such models in generating sequences with the desired function. To illustrate this use case, we guided ProteinMPNN with a large dataset of experimental folding stability measurements on mini-proteins [25] to generate sequences with improved stability. Stability is reported in real-valued units of  $\Delta\Delta G$ , which quantifies the difference in stability from the wild-type sequence. A protein is considered stable if it is at least as stable as the wild-type (*i.e.*,  $\Delta\Delta G \leq 0$ ). To generate sequences with improved stability, we followed the experimental setup from Nisonoff et al. [16]. Specifically, we used ProteinMPNN [1] as the inverse folding model,  $p_\theta(\mathbf{s} | \mathbf{x})$ , where  $\mathbf{s}$  corresponds to a protein sequence and  $\mathbf{x}$  is the desired backbone structure. As described above, the AO-ARM nature of ProteinMPNN means we can treat the pre-trained model as a flow matching / diffusion model,  $p_\theta(\mathbf{s}_1 | \mathbf{s}_t, \mathbf{x})$ , under a masking noise process. Then we apply guidance with the stability predictor from Nisonoff et al. [16],  $p_\phi(\Delta\Delta G | \mathbf{s}, \mathbf{x})$ , to obtain a stability-conditioned inverse folding model,  $p_{\theta,\phi}(\mathbf{s} | \mathbf{x}, \Delta\Delta G \leq 0)$ .

We applied this set-up on the same eight randomly chosen proteins from Nisonoff et al. [16]. For each protein, we sampled 100 sequences using either ProteinMPNN or ProteinMPNN with guidance. For each generated sequence, we define success based on two criteria: (1) the generated sequence should fold into the desired structure,  $\mathbf{x}$ , and (2) the generated sequence should be at least as stable as the wild-type sequence,  $\Delta\Delta G \leq 0$ . We used AlphaFold 2 [76] to predict the structure of the generated sequences and compare the root mean square deviation (RMSD) between the predicted structure and the desired structure  $\mathbf{x}$ . We consider a sequence to achieve the desired fold if the RMSD is less than or equal to  $2\text{\AA}$  following previous evaluation criteria [37]. To evaluate the folding stability of our sequences, we use the  $\Delta\Delta G$  regression model  $p(\Delta\Delta G | \mathbf{s}, \mathbf{x})$ . ProteinMPNN sampling was performed with three different temperatures: 1.0, 0.1, and 0.01 and we report the results for the temperature that achieved the highest success rate. For guided generation, we used a single temperature of 0.1, Euler integration with a step size  $\Delta t = 0.005$ , sampling stochasticity  $\eta = 20$  and guidance strength  $\gamma = 100$  for all proteins. On the whole, we observed that across all proteins, performing guidance with ProteinMPNN consistently improves its success rates (Fig. 2a). Details results are included in the Supplementary Information (Table A1)

## Enzyme class guided sequence generation

### Overview

In this experiment, we demonstrated how guidance can generate sequences from a target enzyme classes under varying levels of sequence constraint. We trained an enzyme class predictor that classifies protein sequences into their Enzyme Commission (EC) numbers based on their sequence and used it to guide the protein language model ESM3 [4] during partial sequence redesign. EC numbers are hierarchical four-level codes describing different enzyme classes.

We use CLEAN [17] to evaluate the generated enzymes as an *in silico* benchmark [59]. This setup enabled us to explore the effectiveness of guidance with different sequence constraints, from complete sequence generation (no constraints) to heavily constrained redesign (50% sequence identity). We additionally present results for EC numbers of varying prevalence in the dataset, measuring generation success of the top-10 most common, 10 random, and 65 rare EC classes.

### Enzyme class predictor

Our enzyme class predictor was a 3-layer multilayer perceptron (MLP) that took mean-pooled ESM3 sequence embeddings as input. The embeddings are of dimension 1536 and we used an MLP with hidden dimension ( $2 * 1536 = 3072$ ).

The model was trained on the SwissProt dataset used by ProteInfer [77]. Unlike CLEAN [17], our model is trained on all SwissProt sequences, including non-enzymes. Sequences for each EC were randomly divided into training and test sets. During method development, we experimented with training classifiers initialized with the CLEAN weights, so the test set did not include any sequences from the CLEAN dataset. The test set contained sequences from ECs with at least 40 samples. At least 30 were used for training, and at most 10 went into the test set, as long as they weren't in the CLEAN training data. Finally, 15% of the non-enzymes were included in the test set, and the rest were used as training data. The training data contained 315,833 samples and the testing data contained 36,354 samples. The noisy predictor's dataset contained 10 randomly sampled noising times for each sequence.

The model was trained with a standard negative log-likelihood objective and an AdamW optimizer (learning rate of 0.001, weight decay coefficient of 0.01). We used a batch size of 15k and trained for two epochs on the full training data. The accuracy curves for each mask-level bin are plotted over the test set of the 100 most common level-4 EC numbers (Fig. A1).

### Experimental setup

For each EC, we sampled 10 wild-type sequences (or as many as possible for rare ECs) from the test set and randomly masked positions according to the target masking level. Then, for each protein in our test set, we created partially masked sequences at 50-100% masked levels (50% is half the sequence fixed and 100% is generated from scratch).

In this experiment, we implemented exact classifier guidance for discrete flow matching as described in Nisonoff et al. [16] using any order sampling as described in Prop. 1. As mentioned in that section, this is similar to the Gillespie algorithm described in Peng et al. [39]. We used a guidance strength  $\gamma = 10$  on the classifier outputs and ESM3 sampling temperature of 0.7. We sampled all positions one at a time.

## Evaluation metrics

We considered the generated sequences a success if CLEAN predicted they belonged to the target enzyme class and if they had a median pLDDT score of at least 0.8, according to the ESM3 structure prediction head.

1. **Functional accuracy:** We used CLEAN to determine if the generated sequence would be classified as belonging to the target EC class. CLEAN encodes the sequence into an embedding and is trained with a contrastive loss. It compares the embedding to a database of reference sequences from each EC class to determine a multi-class classification for each protein. It also produces probability scores with a GMM fit on their validation data. We consider the sequence to be classified correctly if the predicted class is in the set of predicted ECs from CLEAN. We have never seen a CLEAN prediction with more than three classes, although this was not investigated systematically.
2. **Structural plausibility:** We leveraged ESM3’s structure prediction head to assess whether the generated sequences would fold into stable structures. We considered a sequence structurally plausible if its predicted median pLDDT (predicted local distance difference test) score exceeded 0.80.

We analyzed each method’s performance at different masking levels (50%, 60%, 70%, 80%, 90%, and 100%) to understand how the benefit of guidance depends on the level of sequence constraint. This helped us identify regimes where guidance offered significant advantages over unguided generation. We also tested the unguided and conditional models at the 80% level for three different splits of enzyme classes (Table A3). These included: the “Top-10” split of the 10 enzymes classes with the most examples in the test set, the “Random” split of 10 random enzyme classes in the test set, and the “Min-10” split consisting of the 65 most rare classes in the test set (all are among the 100 least prevalent classes in the train set and no class has  $> 20$  training examples).

## Detailed results

The proportion of samples classified by CLEAN to be from the target (specified) enzyme class and the number of these correct samples with median pLDDT  $> 0.8$  were higher when using guidance. When re-designing less than 70% of the sequence, guidance has minimal effect (Fig. 2b). This aligns with the noisy predictor’s performance based on masking level (Fig. A1), where the model’s predictive accuracy plateaus by the 30% unmasking level. Based on these results, we believe guidance only prevents ESM from deviating from the target enzyme class when the sequence is sufficiently close to the target class. However, when more residues must be redesigned, guidance shows a several-fold improvement over the unguided baseline (Table A2). At the 80% masking level, the Random split of 10 random target ECs shows significantly higher success rates than the Top-10 split. For the rare proteins, guidance gets higher CLEAN accuracy, but the pLDDT suffers significantly. The overall success-rate is therefore similar. Full results for each generation test split are in the Supplementary Information (Table A2 and A3).

## Fold class guided backbone generation

### Overview

First, we provide an overview of the experimental set-up for guiding ESM3 backbone structure generation with fold class labels from CATH [26], a hierarchical protein structure classification scheme. This enables both high-level specification of overall secondary structure compositions and more fine-grained descriptions about particular folds. Concretely, we trained a fold classifier,  $p_\phi(\mathbf{c} | \mathbf{x})$  that predict the CATH labels,  $\mathbf{c}$ , from the discrete structure tokens outputted by the structure encoder of ESM3,  $\mathbf{x}$ , on the set of CATH-labeled protein structures from the Protein Data Bank (PDB). We combined this fold class predictor with the structure generation track of ESM3,  $p_\theta(\mathbf{x})$ , to obtain a fold class conditioned backbone structure generative model,  $p_{\theta,\phi}(\mathbf{x} | \mathbf{c})$ .

### Fold classifier

Now we describe additional details of the fold class predictor. Since ESM3 operates on discrete structure tokens, we need a predictor which predicts the fold class label of a protein from its structure token representation. To this end, we first trained a fold class predictor that takes in discrete structure tokens as inputs. The model architecture consists of an encoder-only Transformer trunk. The final per-position embedding is mean-pooled, then fed into three parallel linear layers, each projecting the embedding to a vector with the dimension equal to the number of classes for each of the three levels of CATH hierarchies: C (“Class”), A (“Architecture”) and T (“Topology/Fold”). The C level describes the overall secondary structure-content of a structure (*e.g.*, “mainly  $\alpha$ ”, “mainly  $\beta$ ”, and “mixed  $\alpha/\beta$ ), the A level roughly clusters structures by the overall arrangement of secondary structure in space (*e.g.* “beta barrel”, “roll”), and the T level assigns structures by how the secondary structure elements are connected and arranged (*e.g.* “immunoglobulin-like”, “TIM barrel”) [26]. The model was trained on the PDB dataset following the same pre-processing procedure as in Geffner et al. [18] with a total of 214,564 structures, categorized into 5 C classes, 43 A classes, and 1,336 T classes. We fed each structure through the structure encoder of ESM3 to obtain its structure token representation. The dataset is randomly divided into training, validation, and test sets at a ratio of 8:1:1, ensuring that at least one protein from each class is included in the test set whenever possible.

The model was trained with a standard cross-entropy loss applied to each of the CATH level. Some proteins have multiple CATH labels due to having multiple domains and CATH being a domain-level annotation. For such proteins, we followed Geffner et al. [18] and randomly sampled one domain label as the ground truth for each training iteration, encouraging the model to predict equal probabilities for all domain labels of a protein. During evaluation, if the model predicts any of the correct labels, the prediction is considered correct. For each protein, the loss is calculated for each level of its available CATH label. The transformer trunk of the model has a hidden dimension size of 512, 16 attention heads and 5 encoder layers. In total, the model has around 19 million parameters. The model is trained using the AdamW optimizer [78, 79] with a learning rate of 0.0001, weight decay coefficient of 0.01, a dropout rate of 0.2, a batch size of 128 and a gradient accumulation step of 4. The model is trained for around

26,000 training steps on a single NVIDIA RTX 6000 GPU. We did not systematically tune the hyperparameters of the model. On its test set, the model achieves high accuracies for each level of CATH based on the metrics of Micro Accuracy and Macro Accuracy (Table A4) [80].

The fold classifier used for guidance needs to take in partially masked inputs. We initialized the model weights of this “noisy” classifier with those of the unnoised classifier, and trained it on the same training dataset as the unnoised classifier. We trained the noisy classifier for around 28,000 additional training steps, with the same hyperparameters as the unnoised classifier.

### Fold class guidance

We performed fold class guidance with ESM3 across the three hierarchies of CATH, following the evaluation set-up of Geffner et al. [18]. We sampled backbone structures conditioning on different classes across three levels of the CATH hierarchies. We drew 100 backbone structure samples for each C-level class (mainly  $\alpha$ , mainly  $\beta$ , mixed  $\alpha/\beta$ ), 30 samples for each A-level class, and 30 samples for each of the 30 randomly selected T-level classes, using either the unguided structure generation track of ESM3,  $p_{\theta}(\mathbf{x})$ , or ESM3 with fold class guidance,  $p_{\theta, \phi}(\mathbf{x} | \mathbf{c})$ . For each class, for every sample, we sampled its length uniformly among the lengths present for the proteins of that class in the AFDB, with a minimum length of 50 and maximum length of 275. For unguided generation, we used the default sampling setting of ESM3 with a sampling temperature of 0.7 and  $L$  sampling steps, where  $L$  is the length of the protein sequence. We also experimented with using a lower sampling temperature and found that it results in ESM3 producing predominantly mainly  $\alpha$  proteins. For guided generation, we used a sampling temperature of 0.3, Euler integration with a step size  $\Delta t = 0.005$ , sampling stochasticity  $\eta = 20$  and guidance strength  $\gamma = 100$ . Additional results with different settings of sampling temperatures are in the Supplementary Information (Fig. A3).

We evaluated the generated structures on two criteria: (i) whether the fold classifier,  $p_{\phi}(\mathbf{c} | \mathbf{x})$ , predicts the desired class  $\mathbf{c}$  as the most likely class for the generated structure  $\mathbf{x}$ , and (ii) whether the structures are considered designable, where designability is calculated following the procedure in Yim et al. [81]: for each generated backbone, eight sequences are sampled using ProteinMPNN [1] with a temperature of 0.1, then ESMFold [44] is used to predicted the structure of each generated sequence. The RMSD is calculated between the generated structure and the predicted structure, and a generated backbone is considered designable if the lowest RMSD—referred to as the self-consistency RMSD (scRMSD)—among the eight sampled sequences is  $\leq 2\text{\AA}$ . For the purpose of computing aggregated metrics across multiple classes, we grouped the classes for each level by their frequency of occurrence in AFDB [82] and calculated the classification accuracy and the fraction of designable proteins within each group (Table A5). The frequency groups are defined in the same way as in Geffner et al. [18].

### Detailed results

On the whole, we observed that across all levels and groups, guidance steers generation towards the desired classes (Fig. 2c). Generally, we observed that the classification

accuracy is lower for the A and T level and especially so for the rarer classes. Considering that the A and T level fold class labels are more fine-grained and the constraints are harder to satisfy, and increasingly so for the rarer classes given the imbalanced nature of the fold class distribution, this result is expected. We also observed that among the samples that are classified correctly, only a moderate fraction is designable. This aligns with previous observations that ESM3 tends to produce backbones that are less designable, possibly due to the composition of its training set [18]. We also note that increasing designability does not necessarily correlate with a better capability in generating functional backbone structures, as it has been observed that many functional proteins, *e.g.*, those in the CATH databases, are not designable by the standard definition, and backbone generation models with high designability can systematically miss parts of the structure space that are enriched for these functional proteins [83]. Since guided generation depends crucially on the capability of the underlying unguided model, we can expect structure generation to be improved as better structure generative models are developed. Examples of the generated backbone structures by guiding ESM3 with some example of CATH classes can be found in the Supplementary Information (Fig. A5). The shown examples are both classified correctly to the conditioning fold class by the fold classifier and are designable ( $\text{scRMSD} \leq 2\text{\AA}$ ).

In addition to the metrics of classification accuracy and designability, we also characterized the diversity among the generated structures. We followed Geffner et al. [18] in quantifying diversity by computing the pairwise TM-scores [84] among designable samples stratified by length. TM-scores range from zero to one, where higher scores indicate greater similarity and lower scores means higher diversity among the generated samples. Since we intended to evaluate the quality of the conditional samples, we further filtered the samples to those that are classified correctly to the conditioning fold class by the fold classifier. Since the unguided model rarely sampled structures of the desired class for the A and T level, we only evaluated the diversity of the generated samples when conditioning with classes at the C level. For each C level classes (mainly  $\alpha$ , mainly  $\beta$ , mixed  $\alpha/\beta$ ), we sampled 10,000 structures either with unguided ESM3, or guided with ProteinGuide, and filtered the generated structures to those that are both classified to the desired class by the fold classifier and are designable. We further stratified these samples by length and computed the pairwise TM-scores among the samples for each combination of class and length. The diversity of the generated structures are comparable between the unguided model and that model with ProteinGuide (Fig. A4).

## Guiding base editor for improved editing activity

### Overview

Base editors are engineered CRISPR effectors that can make transition mutations in the DNA by directly deaminating cytosine (causing C-T mutations) or adenine (A-G mutations) in the single-stranded DNA exposed during target recognition by catalytically inactivated Cas9 (dCas9). Adenine base editors (ABEs) can fix about half of the pathogenic point mutations leading to genetic diseases [85]. They have been evolved from an *E.coli* tRNA-deaminase TadA through multiple rounds of directed

evolution [27, 86, 87]. ABEs are compact single domain proteins (167 amino acids) and it has been shown that they can be evolved through at least two different evolutionary trajectories, leading to high DNA deamination activity [27, 87, 88]. Furthermore, both evolutionary paths have led to a high concentrations of mutations in the C-terminal region, suggesting that this region can be a promising target small enough to be chemically synthesized as an oligo pool, but functionally important for evolving DNA base editing activity.

We focused on ABEs because of their importance as an engineering target, their small size and the availability of existing methods for measuring activity based on reversion of an inactivated antibiotic resistance [27, 88] that are suitable for high-throughput screening and detection. Additionally, ABEs (EC 3.5.4.33) are an example of deaminases, a large class of enzymes with important biomedical and biotechnological applications, including other base editors, RNA deaminases and purine and pyrimidine deaminases [89, 90].

We explored how experimental data for base editor activity could be used to condition pre-trained generative models to produce sequences with improved activity. As an overview, we first designed a first-round library with pre-trained generative models. We collected experimental assay-labeled data on each of the designed sequences measuring their activities. Then, we trained a predictor for activity based on the first-round sequences, which we then used to guide the design of a second-round library with ProteinGuide. Our goal was to generate sequences in the second round with improved activities compared to those in the first round.

## ABE Library cloning

ABE libraries contained a diversified region of 86 amino acids (position 82-167) that was synthetically generated as an oligo pool and purchased from Twist Bioscience. The pool was amplified with KAPA polymerase (KAPA HiFi HotStart polymerase, Roche) using the following conditions: 1x KAPA HiFi 2x ReadyMix, 300 nM forward and reverse primer, 5 ng template DNA; 3 min initial denaturation at 95 °C, 20 cycles of 98 °C for 20 sec, 64 °C for 15 sec, 72 °C for 1 min and a final extension of 2 min at 72 °C. The resulting product was loaded on 2% agarose gel and gel-extracted using DNA Clean-Up & Concentration kit (Zymo Research). This pool was then cloned into a vector carrying the rest of the TadA sequence fused to dSpRYCas9 with an XTEN linker following the architecture of ABE0.1 (Supplementary sequence 1) [27]. The library was cloned via Golden Gate assembly using BsaI restriction enzyme and T7 ligase (New England Biolabs). A total of 0.45 pmol library was mixed with 0.15 pmol vector and cycled for 5 min at 37°C and 5 min at 16°C for 30 cycles, followed by 30 min at 37°C and 5 min at 65°C. The assembled library was purified using DNA Clean-Up & Concentration kit (Zymo Research) and transformed in One Shot Top10 competent cells (Thermo Fisher Scientific) by electroporation. 950  $\mu$ L SOC media were added and cells were incubated at 37°C in a shaking incubator at 200 rpm for 1 h. Samples were taken for titer plates to estimate transformation efficiency and the rest of the recovery was inoculated in 2XYT media supplemented with 36  $\mu$ g/mL chloramphenicol and grown for 8h. Plasmid DNA was purified with QIAprep Spin Miniprep Kit (Qiagen) and used for selection experiments.

## Base editing selection assay

To measure adenine base editing we generated a reporter carrying a carbenicillin resistance gene with a stop codon mutation (Supplementary sequence 2) and a corresponding guide RNA and kanamycin resistance gene for plasmid maintainance. The selection strain was produced by transforming Top10 *E.coli* cells with the reporter plasmid and preparing electrocompetent cells. Briefly, the plasmid was transformed in One Shot Top10 (Thermo Fisher Scientific) cells and a single colony was inoculated in liquid culture with 2XYT media and 50  $\mu\text{g}/\text{mL}$  kanamycin. Cells were grown to mid-log phase and spun down at 3500 g, washed twice with ice-cold MiliQ water and twice with 10% glycerol (v/v). Each spin was performed for 10 min at 3500 g and after a final spin of 13 min the cell pellet was resuspended with 2 mL of 10% glycerol for 1 L of starting culture, aliquoted and flash-frozen in liquid nitrogen and stored at  $-80^{\circ}\text{C}$ . For the selection experiments 100  $\mu\text{L}$  of cells were transformed with 200 ng of library plasmid, electroporated and 900  $\mu\text{L}$  of SOC media was added. After 1 h recovery the cells were inoculated in 4 mL 2XYT media supplemented with 50  $\mu\text{g}/\text{mL}$  kanamycin (non-selective antibiotic for the reporter plasmid), 36  $\mu\text{g}/\text{mL}$  chloramphenicol (for the base editor plasmid) and 0.1 % arabinose for induction of the base editor and cells were induced for 20 h (for library 1 experiments) and 16 hours (for library 2). After that cells were washed twice with 2XYT to remove inducer and split in two. Half were inoculated in 30 mL 2XYT with 50  $\mu\text{g}/\text{mL}$  kanamycin and 36  $\mu\text{g}/\text{mL}$  chloramphenicol (non-selective) and the other half inoculated 30 mL 2XYT with 400  $\mu\text{g}/\text{mL}$  carbenicillin and 36  $\mu\text{g}/\text{mL}$  chloramphenicol (selective). Cells were grown to mid to late log phase and spun down, plasmid DNA was isolated using QIAprep Spin Miniprep Kit (Qiagen). 100 ng of the plasmid DNA was used as template for a PCR1 reaction amplifying the variable base editor region and adding adapters for Illumina sequencing (Table A6). The base editor portion was amplified using Q5 polymerase as follows: 100 ng plasmid DNA was used as input, 200 nM forward and reverse primer, 1x Q5 MasterMix. The reaction was carried at  $98^{\circ}\text{C}$  for 30 sec and 20 cycles of  $98^{\circ}\text{C}$  for 10 sec,  $63^{\circ}\text{C}$  for 10 sec and  $72^{\circ}\text{C}$  for 1 min, with a final extension of 5 min at  $72^{\circ}\text{C}$ . The DNA was purified with DNA Clean-Up & Concentration kit (Zymo Research) and sent to Innovative Genomics Institute NGS core facility for PCR2 amplification and sequencing. The library was sequenced with NextSeq 1000/2000 P1 Reagents (300 Cycles) or MiSeq Reagent Kit v2 (600 cycles).

## Processing sequencing data

The paired-end  $2 \times 150$  base pair sequencing reads exhibited variable-length overlapping regions resulting from additional nucleotides incorporated between the Illumina adapters and the primer annealing regions. To process and merge these reads, we first aligned the paired reads to the primer binding sites at both the 5' and 3' termini. In the event of nucleotide call disagreement between the forward and reverse reads in the overlapping region of the two reads, the nucleotide call with the higher Phred score was retained. These merged reads were then matched against the designed library of DNA sequences, keeping only reads with exact matches. To calculate log-enrichments between the selective and non-selective conditions, we added a pseudocount of 1 to all

read counts for both conditions. The log-enrichment,  $\log e_i$ , for each library member indexed by  $i$  was computed as:

$$\log e_i = \log \left( \frac{n_i^s/N^s}{n_i^{ns}/N^{ns}} \right), \quad (37)$$

where  $n_i^s$  and  $n_i^{ns}$  represent the read counts for library member  $i$  in the selective and non-selective conditions, respectively, and  $N^s$  and  $N^{ns}$  denote the total number of read counts in the selective and non-selective conditions, respectively.

## Pre-trained sequence generative models

We hypothesized that the structure of the wild-type TadA protein contains important constraints for maintaining a baseline editing activity, from which we could seek to improve. Therefore, we chose to use sequence generative models that we are able to explicitly condition on the wild-type TadA backbone structure. Specifically, we explored the use of two different pre-trained sequence generative models, ESM3 and FMIF (Flow-Matching Inverse Folding), an inverse folding model which we trained with very similar training data and architecture as ProteinMPNN, but with the explicit flow-matching training objective. We selected FMIF over ProteinMPNN to demonstrate the applicability of our guidance methodology to flow-matching models, thereby establishing the broader generalizability of our approach. For ESM3, we used it as an inverse-folding model by providing the backbone structure as conditioning inputs to the model when generating sequences.

We trained the FMIF model using the same dataset and training protocol described in Nisonoff et al. [16] with two exceptions: (1) we used 3 encoder and decoder layers instead of 4, as both hyperparameter settings performed equally well on a held-out test set and (2) we removed all examples of engineered ABE variants from the 2021 multi-chain training dataset provided by Dauparas et al. [1]. This was done in order to ensure that FMIF does not leverage helpful information for engineering ABEs that is generally not available when engineering a new protein. Specifically, we removed PDB entry 6VPC chains E and F from the training set.

## First-round library design

We built the first-round library by designing two sets of sequences with ESM3 and FMIF separately, then combined the sequences into a pooled library. The wild-type TadA is a homo-dimer, and we sought to adhere to this constraint when generating the sequences. To this end, at each sampling step, we obtained the output logits of the models when conditioning on the structure of homo-dimer. That is, if the protein is of length  $L$ , the output logits is of size  $2L \times S$ , where  $S$  is the alphabet size of the model. We then took the average between the logits which correspond to the same position on sequence of the monomer following Dauparas et al. [1]. We used the averaged logits to parameterize the rate matrix used for sampling. As a result, at each sampling step, we only generate  $L$  residues, one for each position on the monomer, while respecting the structural constraints of the homo-dimer.

In many practical protein engineering applications, it is often desirable to have a control over the number of mutations introduced to the wild-type. In our case, we hoped to have a range of mutation counts in the first-round library, since we do not know a priori how tolerant TadA is to mutations. To this end, we used an additional sampling hyperparameter used in ProteinMPNN [1] which we called the *wild-type weight*,  $w$ . At each sampling step, the output logits of the model is biased by the wild-type weight with  $l_{ds}^w = l_{ds} + w$  for every position  $d$  of the sequence, where  $l_{ds}$  is the original output logits of the model for position  $d$  and state  $s$ , with  $s$  being the state of the wild-type sequence at position  $d$ . Setting  $w = 0$  recovers sampling from the original model, and increasing  $w$  allows one to gradually decrease the number of mutations made to the wild-type sequence, where  $w \rightarrow \infty$  will result in only the wild-type sequence being sampled. The biasing of the logits by the wild-type weight can be interpreted as sampling from a weighted mixture between the original distribution parameterized by the model, and a delta distribution centered on the wild-type sequence. We note that in principle, constraining the number of mutations can also be imposed by introducing a guidance term that encourages the desired number of mutations, but doing so in a computationally tractable way might be challenging, so we leave this investigation to future work.

In our first-round library, we designed around 1,000 sequences with ESM3 and FMIF, respectively, for a total library size of around 2,000 sequences. In addition, we kept three copies of the wild-type TadA sequences in the library as controls. We chose to only design the region of 86 residues on the C-terminal region of the TadA protein due to the cost constraints of gene synthesis, and we hypothesized this region might be enriched for mutations important for increasing editing activity based on prior studies [27], [87], [88]. We fixed active site residues Pro86, Cys87, and Cys90 and allowed the model to design the rest of the region. For both ESM3 and FMIF, we used 8 different values of wild-type weight  $w$  linearly spaced between 0 and 3.5. We sampled from both ESM3 and FMIF using Euler integration with a timestep  $\Delta t = 0.002$ , with a temperature of 0.5 and sampling stochasticity  $\eta = 20$ .

### Predicting ABE activity from the first-round library

The log-enrichment data collected from the first round of designs was used to design a second library enriched in highly-active base editors. Specifically, we sought to generate sequences with an average first-round log-enrichment score of at least 0.0 (Figure A6). To do this, we trained a classifier to predict, given a sequence, whether the sequence’s log-enrichment is greater than zero or not. Guidance requires a classifier trained not only on “clean” / “un-noised” sequence-label pairs,  $\{x_1^i, y^i\}$ , but also trained on “noised” sequence-label pairs  $\{x_t^i, y^i\}$ ,  $t \in [0, 1]$ . This was done in two steps: first, a classifier was trained on just the “un-noised” data and then the classifier was further trained on the “noised” data.

First, the data was pre-processed by discarding sequences with highly-variable log-enrichments between the two replicates. Specifically, any sequences for which the absolute value of the difference in log-enrichments between the two replicates exceeded 0.25 were discarded. This step filtered 114 out of 2,000 sequences. Next, to further mitigate the influence of experimental noise, we discarded sequences with average

log-enrichment scores very close to the class boundary. Specifically, any sequences for which the average log-enrichment was between  $-0.25$  and  $0.25$  were discarded. This step filtered an additional 348 sequences, resulting in a dataset of 132 positive sequences (*i.e.* mean log-enrichment  $\geq 0.25$ ) and 1,406 negative sequences (*i.e.* mean log-enrichment  $\leq -0.25$ ).

Given the relatively small dataset size and significant class imbalance, we implemented a linear classifier augmented with pairwise interaction terms. This approach draws inspiration from Potts models, which are exponential family models that effectively capture pairwise dependencies between positions and have demonstrated robust empirical performance in protein sequence modeling [91]. We trained the model using PyTorch [92, 93], minimizing the binary cross-entropy loss with the AdamW optimizer [78, 79] with a regularization parameter of 10.0 applied specifically to the pairwise interaction terms. Training proceeded for 400 epochs using full-batch gradient descent until convergence of the loss function was observed. Across 10 class-stratified 80%/20% train/validation splits, the model achieved an average validation AUROC of 0.92.

Next, to adapt the classifier to also predict class labels for “noisy” data, we froze all single-site terms involving non-mask tokens as well as any pairwise interaction terms between two non-mask tokens (*i.e.* we only further trained single site parameters corresponding to mask tokens and trained pairwise interaction terms involving at least one mask token). For each gradient step, we first sampled the entire un-noised dataset, then for each sequence in the dataset we randomly sampled a time between 0 and 1, and masked the sequence by sampling from the forward noising process up to that time. The model was again trained for 400 epochs without any regularization, at which point the loss function converged. Training the model in this way, wherein the parameters for the non-mask terms are frozen, has the nice property that the noisy model is guaranteed to be equivalent to the non-noisy model at  $t = 1$ .

## Second-round guided ABE library design

We generated the second-round library by guiding ESM3 and FMIF respectively with the classifier we trained based on the experimental data collected on sequences from the first round. We used the same sampling hyperparameters for each model as we did in the first round, and a guidance factor  $\gamma = 100$ . We designed 944 sequences with each model. All of the generated sequences had a predicted probability of being highly active greater than 0.5. We also included 112 sequences from the first-round library as controls so we could calibrate the log-enrichment measurements between the two rounds. We selected these 112 control sequences with by sampling uniformly across the range of observed log enrichment in the first round.

The 1,888 designed sequences and 112 control sequences were assayed and sequenced with the same protocols as were done in the first round (Figure A7). To enable direct comparison between the first- and second-round libraries, we included 112 sequences from the first round as controls in the second-round library (Figure A8a). These control sequences were selected to span the full range of observed log enrichment values from the first round, providing calibration points across the entire activity spectrum. This design allowed us to quantify and correct for batch effects between the

two experimental rounds. We used these control sequences to learn a linear transformation that maps log enrichment values from the second round to their corresponding values in the first round. Specifically, we fit a linear regression model:

$$\log e_{\text{round 1}} = \alpha \cdot \log e_{\text{round 2}} + \beta \quad (38)$$

where  $\log e_{\text{round 1}}$  and  $\log e_{\text{round 2}}$  represent the log enrichment values for the same sequence in rounds 1 and 2, respectively, and  $\alpha$  (slope) and  $\beta$  (intercept) are the parameters of the linear transformation.

To assess the uncertainty in this calibration procedure, we employed a bootstrap approach using the 112 control sequences. Specifically, we performed 1,000 bootstrap iterations, each time randomly sampling 112 sequences with replacement from our control set and fitting a linear regression model. For each bootstrap sample, we derived a unique set of mapping parameters  $(\alpha_i, \beta_i)$  and used these to transform the entire second-round dataset. We then calculated the median log enrichment value of the transformed second-round sequences for each bootstrap iteration, generating a distribution of potential outcomes that reflects the inherent variability in our experimental measurements. From this distribution of bootstrap outcomes, we identified the 5th and 95th percentile mappings based on the median log enrichment values. These percentiles represent conservative and optimistic estimates, respectively, of the transformation from round 2 to round 1 log enrichment values (Figure A8b).

# Appendix A

## Supplementary tables

**Table A1:** Structure-conditioned protein sequences generation with stability guidance results for all proteins evaluated by predicted stability and folding into correct structure. We defined success as sequences that were generated with  $\text{RMSD} \leq 2\text{\AA}$  and  $\Delta\Delta G \leq 0$ .  $p_\theta(\mathbf{s}|\mathbf{x})$  Temp is the temperature of the baseline structure-conditioned model without stability guidance, while parenthetical  $\gamma$  denotes the guidance strength.

Protein	Method	$p_\theta(\mathbf{s} \mathbf{x})$ Temp	$\Delta\Delta G \leq 0$ % ( $\uparrow$ )	$\text{RMSD} \leq 2\text{\AA}$ % ( $\uparrow$ )	Success % ( $\uparrow$ )
5KPH	ProteinMPNN	1.0	0%	73%	0%
		0.1	6%	100%	6%
		0.01	11%	100%	11%
	+ ProteinGuide ( $\gamma = 100$ )	0.1	100%	100%	100%
1F0M	ProteinMPNN	1.0	0%	96%	0%
		0.1	27%	100%	27%
		0.01	22%	100%	22%
	+ ProteinGuide ( $\gamma = 100$ )	0.1	46%	100%	46%
6M3N	ProteinMPNN	1.0	0%	3%	0%
		0.1	100%	96%	96%
		0.01	99%	98%	97%
	+ ProteinGuide ( $\gamma = 100$ )	0.1	100%	99%	99%
1O6X	ProteinMPNN	1.0	0%	55%	0%
		0.1	47%	100%	47%
		0.01	46%	100%	46%
	+ ProteinGuide ( $\gamma = 100$ )	0.1	96%	100%	96%
2JT1	ProteinMPNN	1.0	0%	87%	0%
		0.1	33%	100%	33%
		0.01	33%	100%	33%
	+ ProteinGuide ( $\gamma = 100$ )	0.1	100%	100%	100%
2JN4	ProteinMPNN	1.0	0%	9%	0%
		0.1	0%	91%	0%
		0.01	0%	93%	0%
	+ ProteinGuide ( $\gamma = 100$ )	0.1	40%	100%	40%
6ACV	ProteinMPNN	1.0	0%	1%	0%
		0.1	0%	64%	0%
		0.01	3%	63%	2%
	+ ProteinGuide ( $\gamma = 100$ )	0.1	38%	57%	24%
2K5N	ProteinMPNN	1.0	0%	81%	0%
		0.1	1%	100%	1%
		0.01	1%	100%	1%
	+ ProteinGuide ( $\gamma = 100$ )	0.1	56%	100%	56%

**Table A2:** Enzyme-class guidance results by masking level for Top-10 most common ECs. Data shown is for 10 wild-type sequences at each masking level for each EC, with one sample for each generation method for each protein. “Mask Level %” is the percent of positions masked, 100 % is full masked. “CLEAN %” is the percentage of samples that were correctly reclassified as the intended target class. “pLDDT > 0.8” is the proportion of samples correctly reclassified by CLEAN that have a median pLDDT across residues above 0.8.

Method	Mask Level %	CLEAN % (†)	Mean pLDDT (†)	pLDDT > 0.8 (†)	Success % (†)
ESM3	100	1%	0.66	0%	0%
	90	30%	0.74	93%	28%
	80	64%	0.84	86%	55%
	70	79%	0.90	92%	73%
	60	77%	0.90	88%	68%
	50	77%	0.89	87%	67%
+ ProteinGuide	100	16%	0.61	60%	10%
	90	53%	0.75	77%	41%
	80	76%	0.85	81%	62%
	70	84%	0.90	90%	76%
	60	89%	0.90	90%	80%
	50	85%	0.90	86%	73%

**Table A3:** Enzyme-class guidance results for different EC sets at 80% masking level. Number of samples (N) per set are indicated. “Mask Level %” is the percent of positions masked, 100 % is full masked. “CLEAN %” is the percentage of samples that were correctly classified as the intended target class. “pLDDT > 0.8” is the proportion of samples correctly reclassified by CLEAN that have a median pLDDT across residues above 0.8.

Method	EC Set	CLEAN % (†)	Mean pLDDT (†)	pLDDT > 0.8 (†)	Success % (†)	N
ESM3	Top-10	64%	0.84	86%	55%	100
	Random	61%	0.83	95%	58%	100
	Min	38%	0.82	94%	36%	86
+ProteinGuide	Top-10	76%	0.85	81%	62%	100
	Random	73%	0.85	99%	72%	100
	Min	41%	0.80	80%	33%	86

**Table A4:** Test set accuracies of the fold classifier used for evaluation in CATH-guided structure generation. Accuracies are computed for each of the CATH level separately. Both Micro and Macro accuracies are reported as alternative ways to average over the different classes within each CATH level [80].

Level	Micro Accuracy (†)	Macro Accuracy (†)
C	0.9888	0.9359
A	0.9678	0.9702
T	0.9490	0.9212

**Table A5:** CATH classes used for conditioning in the fold class guidance experiment, grouped by CATH level and frequency of occurrence in the AFDB. The frequency groups are defined following Geffner et al. [18]. For T level classes, 10 classes are randomly sampled for each of the frequency groups.

CATH Level	Frequency	Classes
<b>A Level</b>	Common (n=9)	2.40, 3.40, 1.20, 1.10, 3.90, 3.30, 3.10, 3.20, 2.60
	Regular (n=13)	2.30, 1.25, 2.170, 4.10, 3.60, 2.20, 3.55, 3.50, 2.130, 2.10, 2.160, 2.70, 2.102
	Rare (n=17)	2.120, 3.15, 2.50, 2.80, 2.100, 1.50, 3.80, 1.40, 3.65, 2.115, 3.75, 3.100, 3.70, 2.110, 2.150, 2.140, 2.90
<b>T Level</b>	Common (n=10)	3.40.190, 2.30.110, 3.40.50, 3.30.70, 3.10.20, 1.10.287, 2.60.40, 1.25.40, 3.10.129, 2.30.30
	Regular (n=10)	1.10.1510, 3.30.1060, 3.90.1030, 1.20.1440, 2.160.10, 3.40.225, 3.30.530, 3.30.429, 3.60.15, 3.10.310
	Rare (n=10)	3.100.10, 2.40.155, 3.30.2430, 3.40.605, 3.30.2370, 1.20.91, 3.90.1470, 3.20.130, 3.90.290, 3.20.190

**Table A6:** Illumina PCR1 primers

Type	Sequence
Forward primers	GCTCTTCCGATCTNCGACGCCACGTTGTAT
	GCTCTTCCGATCTNCGACGCCACGTTGTAT
	GCTCTTCCGATCTNNCGACGCCACGTTGTAT
Reverse primers	GCTCTTCCGATCTNCGCTAGATCCTCCGGA
	GCTCTTCCGATCTNCGCTAGATCCTCCGGA
	GCTCTTCCGATCTNNCGCTAGATCCTCCGGA

## Supplementary figures

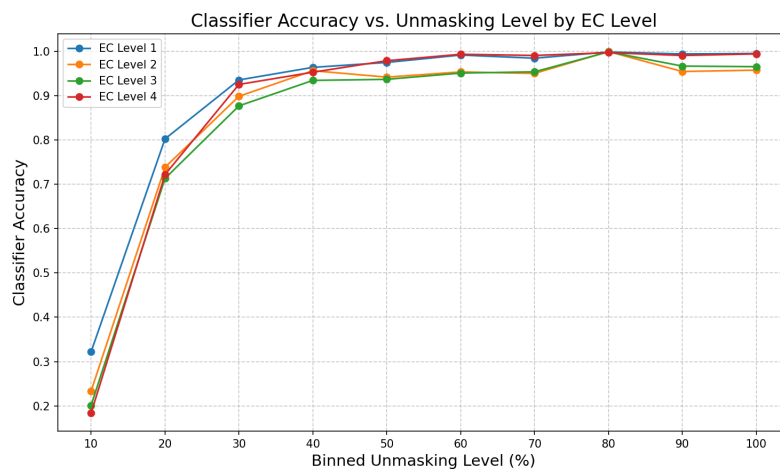


**Fig. A1: Class balanced accuracy of the enzyme classifier on test sequences from the 100 most common level-4 EC classes at different masking levels.** The x-axis shows the masking level from fully masked (left) to fully unmasked (right), while the y-axis shows the balanced accuracy for each of the four EC hierarchical levels.

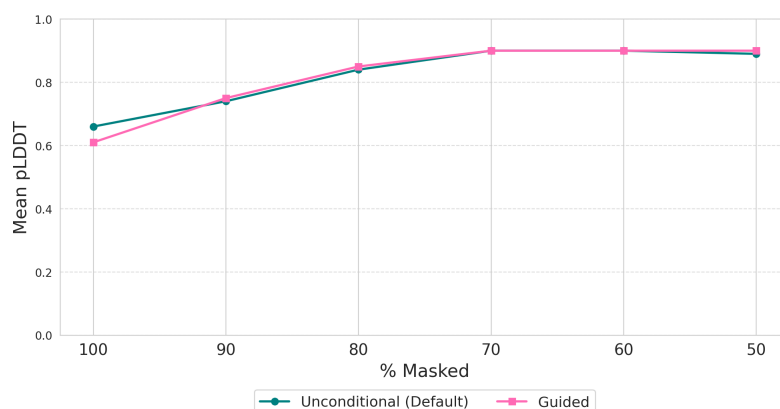


**Fig. A2: Mean pLDDT scores across all samples in the top-10 EC classes experiment.** The plot compares mean pLDDT scores between guided and unconditional generation methods across different masking levels (50%-100%). Higher pLDDT scores indicate better structural confidence in the generated protein sequences, with guided generation consistently producing higher quality structures.



**Fig. A3: Additional fold class generation results with varying sampling temperatures for either ESM3 or ESM3 with ProteinGuide.** The x-axis shows the sampling temperature used with ESM3 when generating backbone structures. The height of each bar shows the percentage of structures correctly classified to their target fold class, while the hatched sub-portion indicates the subset that are also designable (self-consistency RMSD  $\leq 2\text{\AA}$ ). Results are grouped by CATH level (row). For level C (top row), there are three classes: mainly  $\alpha$  (left), mainly  $\beta$  (middle), and mixed  $\alpha/\beta$  (right). For level A (middle row) and T (bottom row), we grouped the classes for each level by their frequency of occurrence in the AFDB into Common (left), Regular (middle), and Rare (right). The metrics were aggregated within each group.

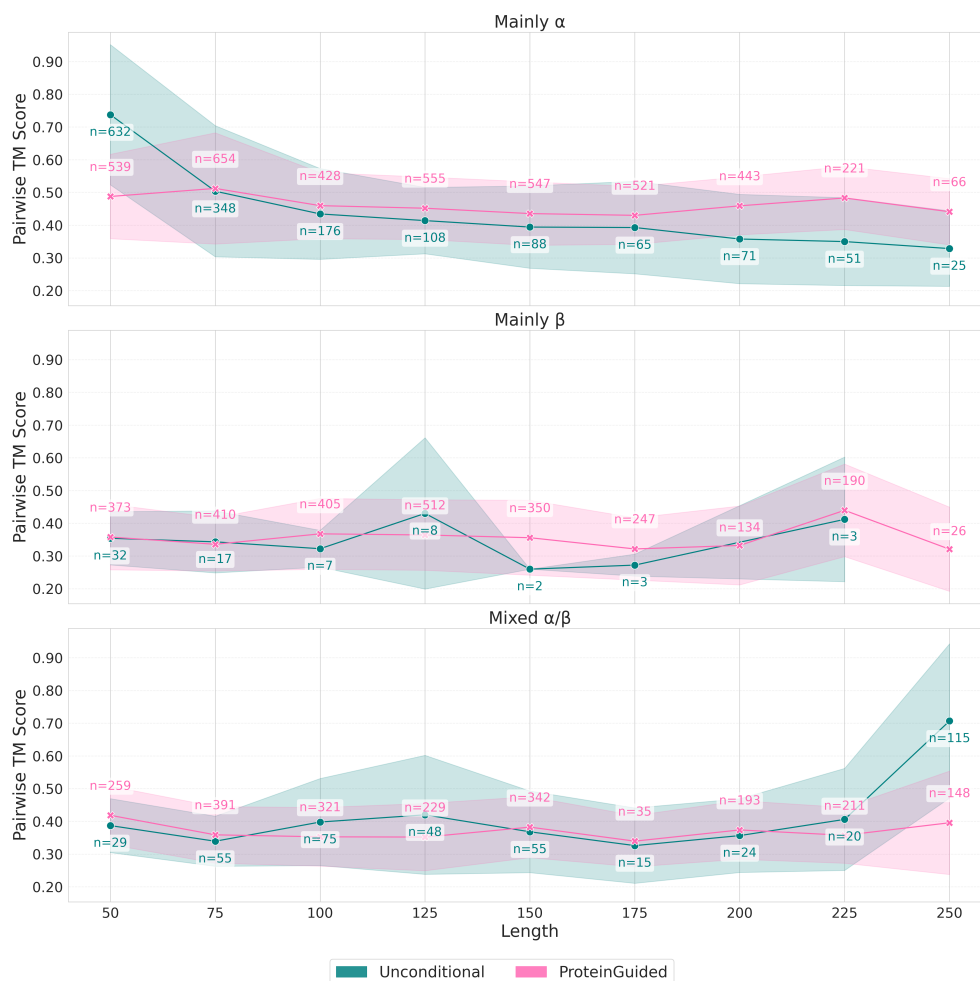


**Fig. A4: Diversity of generated backbone structures for C level, with either ESM3 or ESM3 with ProteinGuide.** Diversity is quantified with TM-scores, which range from zero to one, where lower scores indicate higher diversity. For each C level classes (mainly  $\alpha$ , mainly  $\beta$ , and mixed  $\alpha/\beta$ ), 10,000 structures were sampled, either using unguided ESM3 (teal) or with ProteinGuide (pink). The generated samples were filtered to those that are both classified correctly to the desired fold class by the fold classifier and are designable ( $scRMSD < 2\text{\AA}$ ). These samples were further stratified by length, and the pairwise TM-score was computed among all sampled structures for each combination of class and length. The markers on each line indicate the averaged pairwise TM-score for specific combination of class and length. Error bands represent standard deviation of pairwise TM scores within each length group. The annotated numbers indicate the number of structures that are both classified correctly and designable for each class and length.

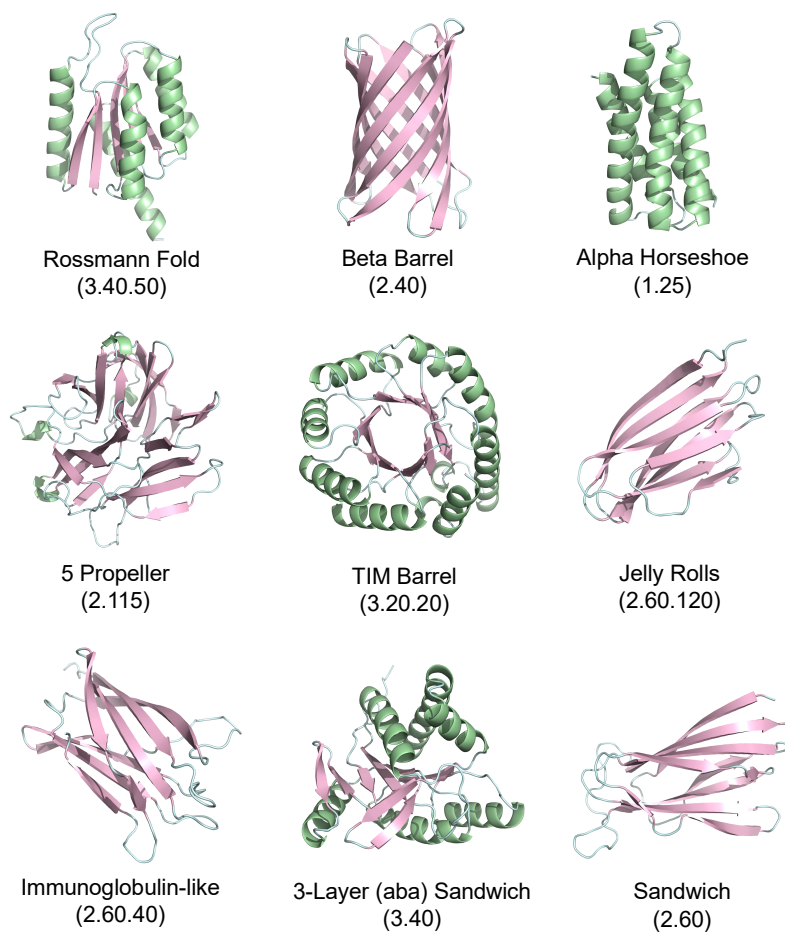


**Fig. A5: Examples of generated protein backbone structures by guiding ESM3 with ProteinGuide to condition on selected examples CATH classes.** The shown proteins are both designable and correctly classified into the desired conditioning fold class. Numbers in parentheses are the corresponding CATH code for the labeled fold classes. Two level digits (*e.g.*, 2.40) represent A level conditioning, and three level digits (*e.g.*, 3.20.20) represent T level conditioning.

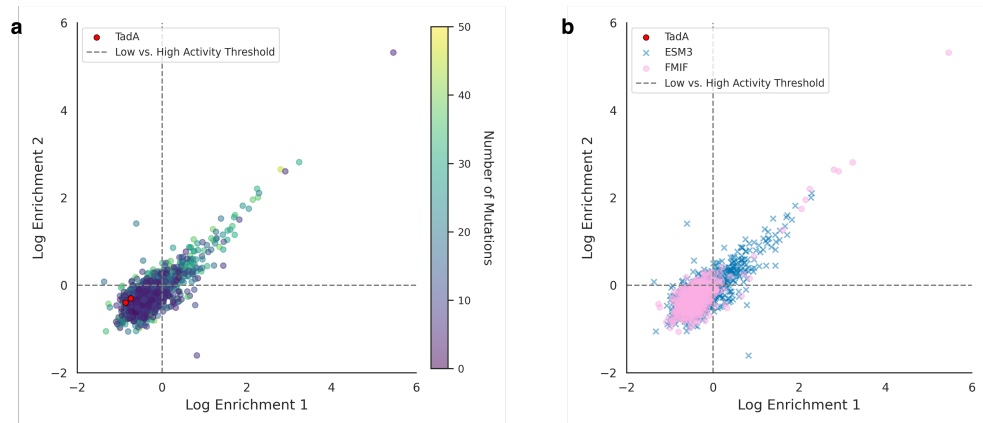


**Fig. A6: Experimental characterization of sequences sampled without ProteinGuide.** **a.** Log enrichment scores of the 2,000 sequences sampled from ESM3 and FMIF for two biological replicates. Each sequence is colored by the number of mutations away from TadA (red). The low vs. high activity threshold used to train a classifier for guidance is shown as a dotted grey line. **b.** The same log enrichment scores as in (a.) but different colors and markers are used to denote which model the sequences were generated from.

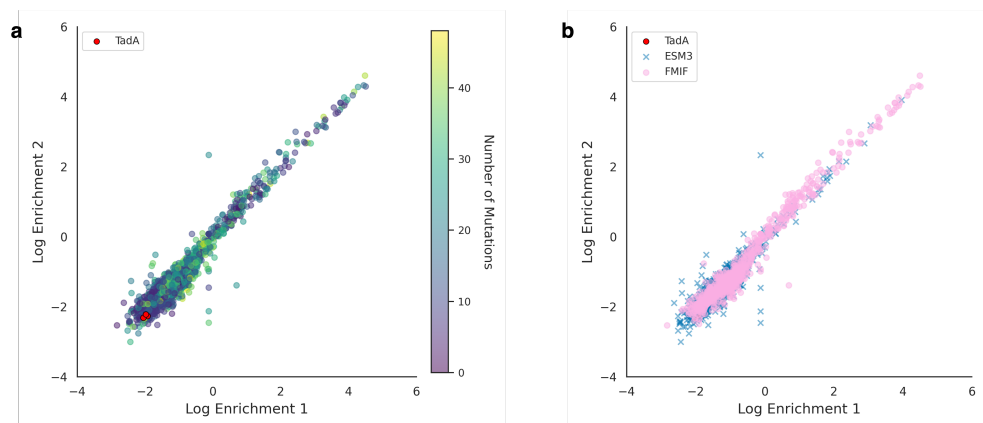


**Fig. A7: Experimental characterization of sequences sampled with ProteinGuide.** **a.** Log enrichment scores of the 1,888 sequences sampled from ESM3 and FMIF with ProteinGuide for two biological replicates. Each sequence is colored by the number of mutations away from TadA (red). **b.** The same log enrichment scores as in (a.) but different colors and markers are used to denote which model the sequences were generated from.

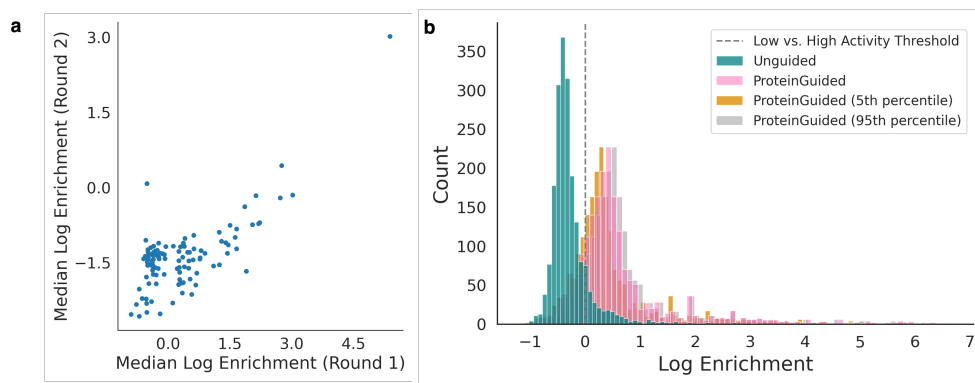


**Fig. A8: Normalizing log enrichment scores between round 1 and round 2**  
**a.** Log enrichment scores of the 112 control sequences that were tested in both round 1 and round 2. The x-axis shows the median log enrichment scores for the replicates from round 1. The y-axis shows the median log enrichment scores for the replicates from round 2. **b.** Histogram of log enrichment values comparing unconditional sequences (teal) and guided sequences (pink) after calibration between rounds. Bootstrap analysis (1,000 iterations) of the 112 control sequences yielded a mean median log enrichment of 0.56 for the guided library with a 90% confidence interval of [0.38, 0.75]. The 5th and 95th percentile mappings (gold and gray histograms, respectively) represent conservative and optimistic transformations based on bootstrap sampling, visualizing the uncertainty range in our calibration procedure. The gray dashed line at a log enrichment value of 0 represents the low vs. high activity classification threshold. Our guidance strategy was designed to generate sequences with log enrichment values greater than this threshold.

Supplementary Sequence 1. TadA-dSpRYCas9 (ABE0.1-SpRY) protein sequence

TadA N-terminal end-TadA diversified region-XTEN linker-dSpRYCas9

MSEVEFSHEYWMRHALTLAKRAWDEREVPVGAVLVHNNRVIGEGWNRPIGRHDPTA  
HAEIMALRQGGLVMQNYRLIDATLYVTLEPCVMCAGAMIHSRIGRVVFGARDAKTGAA  
GSLMDVLHHPGMNHRVEITEGILADECAALLSDFFRMRRQEIKAQKKAQSSTDGGSS  
GGSSGSETPGTSESATPESSGGSSGGSSMDKKYSIGLAIGTNSVGWAVITDEYKVPSK  
FKVLGNTDRHSIKKNLIGALLFDSGETAERTRLRKRTARRRYTRRKNRICYLQEIFSNEMA  
KVDDSFHRLEESFLVEEDKKHERHPIFGNIVDEVAYHEKYPTIYHLRKKLVDSTDKADL  
RLIYLALAHMIKFRGHFLIEGDLNPDNSDVDFIQLVQTYNQLFEENPINASGVDAKAIL  
SARLSKSRLENLIAQLPGEKKNLFGNLIASLGLTPNFKSNFDLAEDAKLQLSKDTYD  
DDLNDLLAQIGDQYADFLAAKNLSDAILSDILRVNTEITKAPLSASMIKRYDEHHQDLT  
LLKALVRQQLPEKYKEIFFDQSKNGYAGYIDGGASQEEFYKFIKPILEKMDGTEELLVKL  
NREDLLRKQRTFDNGSIPHQIHLGELHAILRRQEDFYFPFLKDNREKIEKILTRIPYYVGP  
LARGNSRFAMWTRKSEETITPWNFEVVDKGGASQSFIERMTNFDKNLPNEKVLPHK  
SLLYEYFTVYNELTKVKYVTEGMRKPAFLSGEQKKAIVDLLFKTNRKVTVKQLKEDYFK  
KIECFDSVEISGVEDRFNASLGTYHDLKIIKDKDFLDNEENEDILEDIVLTLTLFEDREMI  
EERLKYAHLFDDKVMKQLKRRRYTGWRLSRKLINGIRDQKQSGKTILDFLKSDGFAN  
RNFMQLIHDDSLTFKEDIQKAQVSGQGDLSLHEHIANLAGSPAIKKGILQTVKVVDELVKL  
MGRHKPENIVIAMARENQTTQKQKNSRERMKRIEIGIKELGSQILKEHPVENTQLQN  
EKLYLYYLQNGRDMYVDQELDINRLSDYDVAIVPQSFLKDDSIDNKVLRSDKNRGGK  
SDNVPSEEVVKKMKNYWRQLLNAKLITQRKFDNLTKAERGGLSELDKAGFIKRQLVET  
RQITKHVAQILD SRMNTKYDENDKLIREVKVITLKSCLVSDFRKDFQFYKVRINNYHHA  
HDAYLNAVVG TALIKYPKLESEFVYGDYKVDVRKMIKSEQEIGKATAKYFFYSNIM  
NFFKTEITLANGEIRKRPLIETNGETGEIVWDKGRDFATVRKVL SMPQVNIVKKTEVQTG  
GFSKESIRPKRNSDKLIARKDWDPKKYGGFLWPTVAYSVLVAKVEKGKSKKLKSVK  
ELLGITIMERSSEFKNPIDFLEAKGYKEVKKDLIIKPKYSLFELENGRKRMLASAKQLQK  
GNELALPSKYVNFLYLASHYEKLGSPEDNEQKQLFVEQHKHYLDEIIIEQISEFSKRVL  
ADANL DKVLSAYNKHDKPIREQAENIIHLFTLTRLGAPRAFKYFDTTIDPKQYRSTKEV  
LDATLIHQISITGLYETRIDLSQLGGD

Fig. A9: Base editor (starting variant) protein sequence

**Supplementary Sequence 2. Carbenicillin resistance gene with Q86Stop mutation**

ATGAGTATTCAACATTTCCGTGTCGCCCTTATTCCCTTTTTGCGGCATTTGCCTT  
CCTGTTTTTGCTCACCCAGAAACGCTGGTGAAAGTAAAAGATGCTGAAGATCAGTT  
GGGTGCACGAGTGGGTTACATCGAACTGGATCTCAACAGCGGTAAGATCCTTGAG  
AGTTTTCGCCCCGAAGAACGTTTTCCAATGATGAGCACTTTTAAAGTTCTGCTATGT  
GGCGCGGTATTATCCCGTATTGACGCCGGGTAAGAGCAACTCGGTGCGCCGCATAC  
ACTATTCTCAGAATGACTTGGTTGAGTACTCACCAGTCACAGAAAAGCATCTTACG  
GATGGCATGACAGTAAGAGAATTATGCAGTGCTGCCATAACCATGAGTGATAACAC  
TGCGGCCAACTTACTTCTGACAACGATCGGAGGACCGAAGGAGCTAACCGCTTTT  
TTGCACAACATGGGGGATCATGTAACCTCGCCTTGATCGTTGGGAACCGGAGCTGA  
ATGAAGCCATACCAAACGACGAGCGTGACACCAGATGCCTGTAGCAATGGCAAC  
AACGTTGCGCAAATACTGCGGAACTACTTACTCTAGCTTCCCGGCAACAAT  
TAATAGACTGGATGGAGGCGGATAAAGTTGCAGGACCATTCTGCGCTCGGCCCT  
TCCGGCTGGCTGGTTTATTGCTGATAAATCTGGAGCCGGTGAGCGTGGGTCTCGC  
GGTATCATTGCAGCACTGGGGCCAGATGGTAAGCCCTCCCGTATCGTAGTTATCTA  
CACGACGGGGAGTCAGGCAACTATGGATGAACGAAATAGACAGATCGCTGAGATA  
GGTGCCTCACTGATTAAGCATTGGTAA

\* Target A (T in the complementary strand)

**Fig. A10: Reporter gene DNA sequence**

## References

- [1] Dauparas, J., Anishchenko, I., Bennett, N., Bai, H., Ragotte, R.J., Milles, L.F., Wicky, B.I., Courbet, A., Haas, R.J., Bethel, N., *et al.*: Robust deep learning-based protein sequence design using ProteinMPNN. *Science* **378**(6615), 49–56 (2022)
- [2] Watson, J.L., Juergens, D., Bennett, N.R., Trippe, B.L., Yim, J., Eisenach, H.E., Ahern, W., Borst, A.J., Ragotte, R.J., Milles, L.F., *et al.*: De novo design of protein structure and function with RFdiffusion. *Nature* **620**(7976), 1089–1100 (2023)
- [3] Ingraham, J.B., Baranov, M., Costello, Z., Barber, K.W., Wang, W., Ismail, A., Frappier, V., Lord, D.M., Ng-Thow-Hing, C., Van Vlack, E.R., *et al.*: Illuminating protein space with a programmable generative model. *Nature* **623**(7989), 1070–1078 (2023)
- [4] Hayes, T., Rao, R., Akin, H., Sofroniew, N.J., Oktay, D., Lin, Z., Verkuil, R., Tran, V.Q., Deaton, J., Wiggert, M., *et al.*: Simulating 500 million years of evolution with a language model. *Science*, 0018 (2025)
- [5] Hsu, C., Verkuil, R., Liu, J., Lin, Z., Hie, B., Sercu, T., Lerer, A., Rives, A.: Learning inverse folding from millions of predicted structures. *ICML* (2022)
- [6] Madani, A., Krause, B., Greene, E.R., Subramanian, S., Mohr, B.P., Holton, J.M., Olmos Jr, J.L., Xiong, C., Sun, Z.Z., Socher, R., *et al.*: Large language models generate functional protein sequences across diverse families. *Nature biotechnology* **41**(8), 1099–1106 (2023)
- [7] Alamdari, S., Thakkar, N., Berg, R., Tenenholtz, N., Strome, B., Moses, A., Lu, A.X., Fusi, N., Amini, A.P., Yang, K.K.: Protein generation with evolutionary diffusion: sequence is all you need. *BioRxiv*, 2023–09 (2023)
- [8] Wang, X., Zheng, Z., Ye, F., Xue, D., Huang, S., Gu, Q.: Diffusion Language Models Are Versatile Protein Learners. In: *International Conference on Machine Learning*, pp. 52309–52333 (2024). PMLR
- [9] Marks, D.S., Colwell, L.J., Sheridan, R., Hopf, T.A., Pagnani, A., Zecchina, R., Sander, C.: Protein 3D structure computed from evolutionary sequence variation. *PloS one* **6**(12), 28766 (2011)
- [10] Russ, W.P., Figliuzzi, M., Stocker, C., Barrat-Charlaix, P., Socolich, M., Kast, P., Hilvert, D., Monasson, R., Cocco, S., Weigt, M., *et al.*: An evolution-based model for designing chorismate mutase enzymes. *Science* **369**(6502), 440–445 (2020)
- [11] Widatalla, T., Rafailov, R., Hie, B.: Aligning protein generative models with experimental fitness via Direct Preference Optimization. *bioRxiv*, 2024–05 (2024)

- [12] Brookes, D., Park, H., Listgarten, J.: Conditioning by adaptive sampling for robust design. In: International Conference on Machine Learning, pp. 773–782 (2019). PMLR
- [13] Sohl-Dickstein, J., Weiss, E., Maheswaranathan, N., Ganguli, S.: Deep Unsupervised Learning using Nonequilibrium Thermodynamics. In: International Conference on Machine Learning, pp. 2256–2265 (2015)
- [14] Dhariwal, P., Nichol, A.: Diffusion Models Beat GANs on Image Synthesis. *Advances in Neural Information Processing Systems* **34**, 8780–8794 (2021)
- [15] Song, Y., Sohl-Dickstein, J., Kingma, D.P., Kumar, A., Ermon, S., Poole, B.: Score-based Generative Modeling through Stochastic Differential Equations. In: International Conference on Learning Representations (2021)
- [16] Nisonoff, H., Xiong, J., Allenspach, S., Listgarten, J.: Unlocking Guidance for Discrete State-Space Diffusion and Flow Models. In: The Thirteenth International Conference on Learning Representations (2025)
- [17] Yu, T., Cui, H., Li, J.C., Luo, Y., Jiang, G., Zhao, H.: Enzyme function prediction using contrastive learning. *Science* **379**(6639), 1358–1363 (2023)
- [18] Geffner, T., Didi, K., Zhang, Z., Reidenbach, D., Cao, Z., Yim, J., Geiger, M., Dallago, C., Kucukbenli, E., Vahdat, A., Kreis, K.: Proteina: Scaling Flow-based Protein Structure Generative Models. In: The Thirteenth International Conference on Learning Representations (2025)
- [19] Austin, J., Johnson, D.D., Ho, J., Tarlow, D., Van Den Berg, R.: Structured Denoising Diffusion Models in Discrete State-Spaces. *Advances in Neural Information Processing Systems* **34**, 17981–17993 (2021)
- [20] Hoogeboom, E., Gritsenko, A.A., Bastings, J., Poole, B., Berg, R., Salimans, T.: Autoregressive Diffusion Models. In: International Conference on Learning Representations (2021). <https://openreview.net/forum?id=Lm8T39vLDTE>
- [21] Shi, J., Han, K., Wang, Z., Doucet, A., Titsias, M.: Simplified and Generalized Masked Diffusion for Discrete Data. *Advances in neural information processing systems* **37**, 103131–103167 (2024)
- [22] Sahoo, S., Arriola, M., Schiff, Y., Gokaslan, A., Marroquin, E., Chiu, J., Rush, A., Kuleshov, V.: Simple and Effective Masked Diffusion Language Models. *Advances in Neural Information Processing Systems* **37**, 130136–130184 (2024)
- [23] Ou, J., Nie, S., Xue, K., Zhu, F., Sun, J., Li, Z., Li, C.: Your Absorbing Discrete Diffusion Secretly Models the Conditional Distributions of Clean Data. In: The Thirteenth International Conference on Learning Representations (2025)

- [24] Yang, K., Klein, D.: FUDGE: Controlled Text Generation With Future Discriminators. In: Proceedings of the 2021 Conference of the North American Chapter of the Association for Computational Linguistics: Human Language Technologies, pp. 3511–3535 (2021)
- [25] Tsuboyama, K., Dauparas, J., Chen, J., Laine, E., Mohseni Behbahani, Y., Weinstein, J.J., Mangan, N.M., Ovchinnikov, S., Rocklin, G.J.: Mega-scale experimental analysis of protein folding stability in biology and design. *Nature* **620**(7973), 434–444 (2023)
- [26] Dawson, N.L., Lewis, T.E., Das, S., Lees, J.G., Lee, D., Ashford, P., Orengo, C.A., Sillitoe, I.: CATH: an expanded resource to predict protein function through structure and sequence. *Nucleic acids research* **45**(D1), 289–295 (2017)
- [27] Gaudelli, N.M., Komor, A.C., Rees, H.A., Packer, M.S., Badran, A.H., Bryson, D.I., Liu, D.R.: Programmable base editing of A•T to G•C in genomic DNA without DNA cleavage. *Nature* **551**(7681), 464–471 (2017)
- [28] Ranzau, B.L., Rallapalli, K.L., Evanoff, M., Paesani, F., Komor, A.C.: The Wild-Type tRNA Adenosine Deaminase Enzyme TadA Is Capable of Sequence-Specific DNA Base Editing. *ChemBioChem* **24**(16), 202200788 (2023)
- [29] Ho, J., Jain, A., Abbeel, P.: Denoising Diffusion Probabilistic Models. *Advances in Neural Information Processing Systems* **33**, 6840–6851 (2020)
- [30] Hooeboom, E., Nielsen, D., Jaini, P., Forré, P., Welling, M.: Argmax Flows and Multinomial Diffusion: Learning Categorical Distributions. *Advances in Neural Information Processing Systems* **34**, 12454–12465 (2021)
- [31] Campbell, A., Benton, J., De Bortoli, V., Rainforth, T., Deligiannidis, G., Doucet, A.: A Continuous Time Framework for Discrete Denoising Models. *Advances in Neural Information Processing Systems* **35**, 28266–28279 (2022)
- [32] Sun, H., Yu, L., Dai, B., Schuurmans, D., Dai, H.: Score-based Continuous-time Discrete Diffusion Models. In: International Conference on Learning Representations (2023)
- [33] Lou, A., Meng, C., Ermon, S.: Discrete Diffusion Language Modeling by Estimating the Ratios of the Data Distribution. *arXiv:2310.16834* (2023)
- [34] Albergo, M.S., Vanden-Eijnden, E.: Building Normalizing Flows with Stochastic Interpolants. In: International Conference on Learning Representations (2023)
- [35] Lipman, Y., Chen, R.T.Q., Ben-Hamu, H., Nickel, M., Le, M.: Flow Matching for Generative Modeling. In: International Conference on Learning Representations (2023)

- [36] Liu, X., Gong, C., Liu, Q.: Flow Straight and Fast: Learning to Generate and Transfer Data with Rectified Flow. In: International Conference on Learning Representations (2023)
- [37] Campbell, A., Yim, J., Barzilay, R., Rainforth, T., Jaakkola, T.S.: Generative Flows on Discrete State-Spaces: Enabling Multimodal Flows with Applications to Protein Co-Design. In: International Conference on Machine Learning (2024)
- [38] Gat, I., Remez, T., Shaul, N., Kreuk, F., Chen, R.T., Synnaeve, G., Adi, Y., Lipman, Y.: Discrete flow matching. In: Advances in Neural Information Processing Systems, vol. 37 (2024)
- [39] Peng, F.Z., Bezemek, Z., Patel, S., Rector-Brooks, J., Yao, S., Tong, A., Chatterjee, P.: Path planning for masked diffusion model sampling. arXiv preprint arXiv:2502.03540 (2025)
- [40] Gillespie, D.T.: Exact stochastic simulation of coupled chemical reactions. The Journal of Physical Chemistry **81**(25), 2340–2361 (1977)
- [41] Gillespie, D.T.: Approximate accelerated stochastic simulation of chemically reacting systems. The Journal of Physical Chemistry **115**(4), 1716–1733 (2001)
- [42] Uria, B., Murray, I., Larochelle, H.: A deep and tractable density estimator. In: International Conference on Machine Learning, pp. 467–475 (2014). PMLR
- [43] Chang, H., Zhang, H., Jiang, L., Liu, C., Freeman, W.T.: Maskgit: Masked generative image transformer. In: Proceedings of the IEEE/CVF Conference on Computer Vision and Pattern Recognition, pp. 11315–11325 (2022)
- [44] Lin, Z., Akin, H., Rao, R., Hie, B., Zhu, Z., Lu, W., Smetanin, N., Verkuil, R., Kabeli, O., Shmueli, Y., *et al.*: Evolutionary-scale prediction of atomic-level protein structure with a language model. Science **379**(6637), 1123–1130 (2023)
- [45] Ho, J., Salimans, T.: Classifier-Free Diffusion Guidance. In: Neural Information Processing Systems - Workshop on Deep Generative Models and Downstream Applications (2021)
- [46] Karras, T., Aittala, M., Kynkäänniemi, T., Lehtinen, J., Aila, T., Laine, S.: Guiding a diffusion model with a bad version of itself. Advances in Neural Information Processing Systems **37**, 52996–53021 (2024)
- [47] Grathwohl, W., Swersky, K., Hashemi, M., Duvenaud, D., Maddison, C.: Oops I Took a Gradient: Scalable Sampling for Discrete Distributions. In: International Conference on Machine Learning, pp. 3831–3841 (2021)
- [48] Wu, L., Trippe, B., Naesseth, C., Blei, D., Cunningham, J.P.: Practical and asymptotically exact conditional sampling in diffusion models. Advances in Neural

- [49] Li, X., Zhao, Y., Wang, C., Scalia, G., Eraslan, G., Nair, S., Biancalani, T., Ji, S., Regev, A., Levine, S., et al.: Derivative-free guidance in continuous and discrete diffusion models with soft value-based decoding. arXiv preprint arXiv:2408.08252 (2024)
- [50] Schiff, Y., Sahoo, S.S., Phung, H., Wang, G., Boshar, S., Dalla-torre, H., Almeida, B.P., Rush, A.M., PIERROT, T., Kuleshov, V.: Simple Guidance Mechanisms for Discrete Diffusion Models. In: The Thirteenth International Conference on Learning Representations (2025)
- [51] Singhal, R., Horvitz, Z., Teehan, R., Ren, M., Yu, Z., McKeown, K., Ranganath, R.: A general framework for inference-time scaling and steering of diffusion models. arXiv preprint arXiv:2501.06848 (2025)
- [52] Lee, C.K., Jeha, P., Frelsen, J., Lio, P., Albergo, M.S., Vargas, F.: Debiasing guidance for discrete diffusion with sequential monte carlo. arXiv preprint arXiv:2502.06079 (2025)
- [53] Du, Y., Durkan, C., Strudel, R., Tenenbaum, J.B., Dieleman, S., Fergus, R., Sohl-Dickstein, J., Doucet, A., Grathwohl, W.S.: Reduce, Reuse, Recycle: Compositional Generation with Energy-Based Diffusion Models and MCMC. In: International Conference on Machine Learning, pp. 8489–8510 (2023)
- [54] Zhao, S., Brekelmans, R., Makhzani, A., Grosse, R.: Probabilistic inference in language models via twisted sequential monte carlo. arXiv preprint arXiv:2404.17546 (2024)
- [55] Wang, C., Uehara, M., He, Y., Wang, A., Lal, A., Jaakkola, T., Levine, S., Regev, A., Hanchen, Biancalani, T.: Fine-Tuning Discrete Diffusion Models via Reward Optimization with Applications to DNA and Protein Design. In: The Thirteenth International Conference on Learning Representations (2025)
- [56] Rector-Brooks, J., Hasan, M., Peng, Z., Liu, C.-H., Mittal, S., Dziri, N., Bronstein, M.M., Chatterjee, P., Tong, A., Bose, J.: Steering masked discrete diffusion models via discrete denoising posterior prediction. In: The Thirteenth International Conference on Learning Representations (2025)
- [57] Rafailov, R., Sharma, A., Mitchell, E., Manning, C.D., Ermon, S., Finn, C.: Direct preference optimization: Your language model is secretly a reward model. *Advances in Neural Information Processing Systems* **36**, 53728–53741 (2023)
- [58] Chennakesavalu, S., Hu, F., Ibarraran, S., Rotskoff, G.M.: Aligning chemical and protein language models with continuous feedback using energy rank alignment. In: ICLR 2025 Workshop on Generative and Experimental Perspectives for Biomolecular Design (2025)

- [59] Stocco, F., Artigues-Lleixa, M., Hunklinger, A., Widatalla, T., Guell, M., Ferruz, N.: Guiding Generative Protein Language Models with Reinforcement Learning. arXiv preprint arXiv:2412.12979 (2024)
- [60] Wallace, B., Dang, M., Rafailov, R., Zhou, L., Lou, A., Purushwalkam, S., Ermon, S., Xiong, C., Joty, S., Naik, N.: Diffusion model alignment using direct preference optimization. In: Proceedings of the IEEE/CVF Conference on Computer Vision and Pattern Recognition, pp. 8228–8238 (2024)
- [61] Borso, U., Paglieri, D., Wells, J., Rocktäschel, T.: Preference-Based Alignment of Discrete Diffusion Models. In: ICLR 2025 Workshop on Bidirectional Human-AI Alignment (2025)
- [62] Yang, J., Chu, W., Khalil, D., Astudillo, R., Wittmann, B.J., Arnold, F.H., Yue, Y.: Steering Generative Models with Experimental Data for Protein Fitness Optimization (2025). <https://arxiv.org/abs/2505.15093>
- [63] Schulman, J., Wolski, F., Dhariwal, P., Radford, A., Klimov, O.: Proximal policy optimization algorithms. arXiv preprint arXiv:1707.06347 (2017)
- [64] Blalock, N., Seshadri, S., Babbar, A., Fahlberg, S.A., Kulkarni, A., Romero, P.A.: Functional alignment of protein language models via reinforcement learning. bioRxiv, 2025–05 (2025)
- [65] Avdeyev, P., Shi, C., Tan, Y., Dudnyk, K., Zhou, J.: Dirichlet Diffusion Score Model for Biological Sequence Generation. In: International Conference on Machine Learning, pp. 1276–1301 (2023). <https://proceedings.mlr.press/v202/avdeyev23a/avdeyev23a.pdf>
- [66] Li, X., Thickstun, J., Gulrajani, I., Liang, P.S., Hashimoto, T.B.: Diffusion-LM Improves Controllable Text Generation. Advances in Neural Information Processing Systems **35**, 4328–4343 (2022)
- [67] Dieleman, S., Sartran, L., Roshannai, A., Savinov, N., Ganin, Y., Richemond, P.H., Doucet, A., Strudel, R., Dyer, C., Durkan, C., et al.: Continuous diffusion for categorical data. arXiv:2211.15089 (2022)
- [68] Gruver, N., Stanton, S., Frey, N., Rudner, T.G., Hotzel, I., Lafrance-Vanasse, J., Rajpal, A., Cho, K., Wilson, A.G.: Protein Design with Guided Discrete Diffusion. Advances in Neural Information Processing Systems **36** (2024)
- [69] Lisanza, S.L., Gershon, J.M., Tipps, S.W., Sims, J.N., Arnoldt, L., Hendel, S.J., Simma, M.K., Liu, G., Yase, M., Wu, H., et al.: Multistate and functional protein design using rosettafold sequence space diffusion. Nature biotechnology, 1–11 (2024)
- [70] Chen, Z., Yuan, H., Li, Y., Kou, Y., Zhang, J., Gu, Q.: Fast sampling via discrete

- non-markov diffusion models with predetermined transition time. *Advances in Neural Information Processing Systems* **37**, 106870–106905 (2024)
- [71] Zheng, K., Chen, Y., Mao, H., Liu, M.-Y., Zhu, J., Zhang, Q.: Masked diffusion models are secretly time-agnostic masked models and exploit inaccurate categorical sampling. *arXiv preprint arXiv:2409.02908* (2024)
- [72] Ou, J., Nie, S., Xue, K., Zhu, F., Sun, J., Li, Z., Li, C.: Your absorbing discrete diffusion secretly models the conditional distributions of clean data. *arXiv preprint arXiv:2406.03736* (2024)
- [73] Yang, Z., Dai, Z., Yang, Y., Carbonell, J., Salakhutdinov, R.R., Le, Q.V.: Xlnet: Generalized autoregressive pretraining for language understanding. *Advances in neural information processing systems* **32** (2019)
- [74] Strauss, R., Oliva, J.B.: Arbitrary conditional distributions with energy. *Advances in Neural Information Processing Systems* **34**, 752–763 (2021)
- [75] Del Moral, P., Penev, S.: *Stochastic Processes: From Applications to Theory*. Chapman and Hall/CRC, ??? (2017)
- [76] Jumper, J., Evans, R., Pritzel, A., Green, T., Figurnov, M., Ronneberger, O., Tunyasuvunakool, K., Bates, R., Židek, A., Potapenko, A., *et al.*: Highly accurate protein structure prediction with AlphaFold. *Nature* **596**(7873), 583–589 (2021)
- [77] Sanderson, T., Bileschi, M.L., Belanger, D., Colwell, L.J.: Proteinfer, deep neural networks for protein functional inference. *Elife* **12**, 80942 (2023)
- [78] Kingma, D.P., Ba, J.: Adam: A Method for Stochastic Optimization. In: *International Conference on Learning Representations (ICLR)* (2015)
- [79] Loshchilov, I., Hutter, F.: Decoupled Weight Decay Regularization. In: *International Conference on Learning Representations* (2019)
- [80] Grandini, M., Bagli, E., Visani, G.: Metrics for multi-class classification: an overview. *arXiv preprint arXiv:2008.05756* (2020)
- [81] Yim, J., Trippe, B.L., De Bortoli, V., Mathieu, E., Doucet, A., Barzilay, R., Jaakkola, T.: SE (3) Diffusion Model with Application to Protein Backbone Generation. In: *International Conference on Machine Learning*, pp. 40001–40039 (2023). PMLR
- [82] Varadi, M., Anyango, S., Deshpande, M., Nair, S., Natassia, C., Yordanova, G., Yuan, D., Stroe, O., Wood, G., Laydon, A., *et al.*: Alphafold protein structure database: massively expanding the structural coverage of protein-sequence space with high-accuracy models. *Nucleic acids research* **50**(D1), 439–444 (2022)
- [83] Lu, T., Liu, M., Chen, Y., Kim, J., Huang, P.-S.: Assessing Generative Model

Coverage of Protein Structures with SHAPES. bioRxiv, 2025–01 (2025)

- [84] Zhang, Y., Skolnick, J.: Scoring function for automated assessment of protein structure template quality. *Proteins: Structure, Function, and Bioinformatics* **57**(4), 702–710 (2004)
- [85] Rees, H.A., Liu, D.R.: Base editing: precision chemistry on the genome and transcriptome of living cells. *Nature reviews genetics* **19**(12), 770–788 (2018)
- [86] Gaudelli, N.M., Lam, D.K., Rees, H.A., Solá-Esteves, N.M., Barrera, L.A., Born, D.A., Edwards, A., Gehrke, J.M., Lee, S.-J., Liquori, A.J., *et al.*: Directed evolution of adenine base editors with increased activity and therapeutic application. *Nature biotechnology* **38**(7), 892–900 (2020)
- [87] Richter, M.F., Zhao, K.T., Eton, E., Lapinaite, A., Newby, G.A., Thuronyi, B.W., Wilson, C., Koblan, L.W., Zeng, J., Bauer, D.E., *et al.*: Phage-assisted evolution of an adenine base editor with improved Cas domain compatibility and activity. *Nature biotechnology* **38**(7), 883–891 (2020)
- [88] Xiao, Y.-L., Wu, Y., Tang, W.: An adenine base editor variant expands context compatibility. *Nature Biotechnology* **42**(9), 1442–1453 (2024)
- [89] Budzko, L., Hoffa-Sobiech, K., Jackowiak, P., Figlerowicz, M.: Engineered deaminases as a key component of DNA and RNA editing tools. *Molecular Therapy Nucleic Acids* **34**, 102062 (2023)
- [90] Del Arco, J., Acosta, J., Fernández-Lucas, J.: Biotechnological applications of purine and pyrimidine deaminases. *Biotechnology Advances* **77**, 108473 (2024)
- [91] Hopf, T.A., Ingraham, J.B., Poelwijk, F.J., Schärfe, C.P., Springer, M., Sander, C., Marks, D.S.: Mutation effects predicted from sequence co-variation. *Nature biotechnology* **35**(2), 128–135 (2017)
- [92] Paszke, A., Gross, S., Massa, F., Lerer, A., Bradbury, J., Chanan, G., Killeen, T., Lin, Z., Gimelshein, N., Antiga, L., *et al.*: PyTorch: An Imperative Style, High-Performance Deep Learning Library. *Advances in Neural Information Processing Systems*, 8024–8035
- [93] Ansel, J., Yang, E., He, H., Gimelshein, N., Jain, A., Voznesensky, M., Bao, B., Bell, P., Berard, D., Burovski, E., *et al.*: Pytorch 2: Faster machine learning through dynamic python bytecode transformation and graph compilation. In: *Proceedings of the 29th ACM International Conference on Architectural Support for Programming Languages and Operating Systems*, Volume 2, pp. 929–947 (2024)